Influence of salt-related mechanical layering on the seismic potential of active faults: Insights from the southwestern Valencia Trough (W Mediterranean)

Iván Martin-Rojas[1]

Adrià Ramos[2, 1]

Menno De Ruig [2]

Iván Medina-Cascales[1]

Eva Santamaría-Pérez[1]

Pedro Alfaro[1]

1 Dpto. de Ciencias de la Tierra y del Medio Ambiente, Universidad de Alicante, Campus San Vicente s/n, 03690, San Vicente del Raspeig, Alicante. ivan.martin@ua.es

2. Departament de Botànica i Geologia, Universitat de València, 46010 Burjassot, Valencia, Spain

3. Lithologic, 2582 LD The Hague, The Netherlands. lithologic.mail@gmail.com

Corresponding author: Martin-Rojas, Iván

Dpto. de Ciencias de la Tierra y del Medio Ambiente, Universidad de Alicante, Campus San Vicente s/n, 03690, San Vicente del Raspeig, Alicante. ivan.martin@ua.es

Short summary

This study investigates the main active faults located within the southwestern Valencia Trough, an offshore region east of the Spanish coast. Utilizing subsurface data, we identify and characterize the 3D geometry of several of these faults for the first time. Given that active faults pose a significant natural hazard owing to their potential to generate earthquakes, we also assess the seismic potential of the faults within the southwestern Valencia Trough.

ABSTRACT

We present a structural and seismotectonic analysis of active faults in the southwestern Valencia Trough (western Mediterranean) on the basis of subsurface datasets. In our study, we identify and characterise three major active faults: the Cullera Fault, with long-term slip rates that vary over time between 0.15 ± 0.1 mm/yr and 0.4 ± 0.1 mm/yr; the oblique Albufera Fault, with a long-term slip rate of 0.2 ± 0.1 mm/yr; and the normal Valencia Fault.

The seismogenic character of the southwestern Valencia Trough is controlled by a mechanically weak layer consisting of Triassic evaporites. This weak layer induces partial-to-complete decoupling between the suprasalt and subsalt successions, leading to two distinct mechanisms driving fault displacement: tectonic activity and salt withdrawal. A quantitative evolutionary analysis of the Cullera Fault reveals that these two mechanisms occur alternately over time.

The presence of a mechanically weak layer has implications for seismicity. Earthquakes can nucleate within both sub- and suprasalt successions, with total or partial decoupling influencing rupture propagation. We discuss how these two scenarios lead to different earthquakes and thus impact the seismic hazard of a region. Empirical source-scaling relationships, which are commonly used to estimate the seismogenic potential of active faults, generally assume a homogeneous seismogenic crust. To address this limitation, we propose a methodological approach based on the use of the aspect ratio. Using this method, the maximum magnitudes for suprasalt ruptures are 5.8-6.4, 5.4-6.2, and 5.1-5.9 for the Cullera, Valencia, and Albufera faults, respectively. These values are 11-25% lower than those obtained by considering the rupture of the entire seismogenic crust. Our findings highlight the need to incorporate stratigraphic mechanical layering into seismic hazard assessments, particularly in salt-influenced tectonic settings.

1. Introduction

Seismic hazard analyses are often performed by scaling relationships. These relationships are regressions in which the seismogenic potential of active faults is derived from geometric parameters of the fault, such as the potential fault rupture length or area (Stirling et al., 2013). Pioneering works on scaling relationships began in the 1970s (Kanamori & Anderson, 1975; Geller, 1976). The regressions of Wells & Coppersmith (1994) represent a milestone in the application of scaling relationships, as they included a very large dataset of historical earthquakes. The equations proposed by Wells & Coppersmith became a standard for determining the seismogenic potential of active faults. Subsequently, other scaling relationships have been proposed, accounting for factors such as the tectonic environment, fault dip, or seismogenic thickness (Stirling et al., 2002 and 2013; Leonard 2010 and 2014; Huang et al., 2024, among many others).

Most scaling relationships employed to evaluate crustal earthquakes correlate the moment magnitude (Mw) with the fault dimensions (length, width, and/or area). Some of these scaling relationships consider the fault width vs. fault dip growth of ruptures for large earthquakes, as rupture width is limited by the maximum depth of the seismogenic crust (Leonard, 2010; Yen and Ma, 2011; Leonard, 2014; Cheng et al., 2019). Standard relationships include data from hundreds or even thousands of events. Therefore, the influence in these relationships of potential mechanical heterogeneities within the seismogenic crust should be implicit. However, because of the large amount of data, the mean regressions average out the less common situations, as the presence of a mechanical weak layer. Therefore, as a consequence of this averaging, the empirical relationships do not permit to compute the influence of potential heterogeneities within the seismogenic crust. These heterogeneities could control the vertical propagation of ruptures and, therefore, the magnitude of earthquakes.

Here, we present an analysis of several subsurface datasets, including high-resolution seismic profiles, from the southwestern Valencia Trough. We identify and characterise the main active faults in this region, and we carry out a detailed geometric description. The results of this analysis also emphasize that this region is

characterised by a mechanically weak layer within the seismogenic crust. After mapping the main faults, we apply conventional scaling relationships to evaluate the potential magnitudes of future earthquakes. We propose a methodological approach for integrating the effects of mechanically weak layers—such as Triassic evaporites—into routine seismic hazard assessments, highlighting the need to refine existing scaling relationships in tectonically complex settings.

2. Tectonic setting

The Valencia Trough is an extensional basin located in the western Mediterranean region (Fig. 1). This basin is the result of polyphase tectonic evolution spanning from the Triassic to the present day, as it is located between the Betic–Balearic fold-and-thrust belt to the south, the Iberian Chain to the west, and the Catalan Coastal Range to the north (De Ruig, 1992; Guimerà & Álvaro, 1990; Maillard & Mauffret, 1999; Roca & Desegaulx, 1992; Roca et al., 2004; Vergés & Fernàndez, 2012). The tectonic evolution of the Valencia Trough is also partially influenced by extension related to the retreat of the Maghrebian–Ligurian Tethys subduction slab (Etheve et al., 2016; Faccenna et al., 2004; Jolivet & Faccenna, 2000; Maillard & Mauffret, 1999; Rehault et al., 1984; Roca et al., 1999; Séranne, 1999; van Hinsbergen et al., 2014).

The Valencia Trough (Fig. 1) underwent a Mesozoic rifting process related to the Iberian intraplate rift and the opening of the Western Tethys (Arche and López-Gómez, 1996; Nebot and Guimerà, 2018; Ramos et al., 2023; Salas et al., 2001). This process led to the formation of NW–SE and NE–SW high-angle faults offsetting the pre-Mesozoic basement and to the deposition of a 5–15-km-thick Upper Jurassic-Lower Cretaceous succession.

During the Late Cretaceous, the onset of convergence between Nubia and Eurasia caused the transition from a Mesozoic extensional tectonic regime to successive compressional and extensional stages (Roca, 2001; Salas et al., 2001; Vergés and Sàbat, 1999). From the late Eocene to the Oligocene, the Valencia Trough was dominated by shortening. Onshore, this episode led to the formation of the intraplate Iberian Chain and Catalan Coastal Ranges (Gaspar-Escribano et al., 2004; Geel, 1995; Guimerà and Álvaro, 1990).

From the late Oligocene to the middle Miocene, the western Mediterranean region was subsequently affected by an extensional regime, driven by the complex interplay between the European–Cenozoic rift system (e.g., Séranne, 1999) and the rollback of the Maghrebian–Ligurian Tethys slab (Faccenna et al., 2004; van Hinsbergen et al., 2014). This extensional phase led to the formation of the Liguro-Provençal and Algerian Basins, as well as the Valencia Trough. However, subsidence in the southwestern Valencia Trough during this period cannot be accounted for by

rifting, due to the limited occurrence of Cenozoic basement extensional faults (Roca and Guimerà, 1992). Therefore, extension has been interpreted as due to the collapse of a back-arc transient uplift event (Fang et al., 2021).

The extension in the Valencia Trough occurred immediately before or synchronously with the formation of the compressional Betic Cordillera. This compressional deformation is well expressed by a thin-skinned fold-and-thrust system observed in the Eastern Betic Cordillera (De Ruig, 1995; Sàbat et al., 2011) and in the Balearic Promontory (Mallorca and Ibiza Islands). At the same time, significant magmatic activity took place in the area. This magmatism was divided into two phases: (1) late Oligocene to Serravallian calc-alkaline activity and (2) Tortonian to present alkaline volcanic activity (Martí et al., 1992).

From the Pliocene to the present, the tectonic setting in the Valencia Trough has been dominated by NE–SW extension, as indicated by focal mechanisms (Stich et al., 2010) and broad regional global navigation satellite system (GNSS) analyses (Stich et al., 2006). This extension has been related to thermal subsidence (Roca, 1992, 1996, and 2001; Roca and Guimerà, 1992; Roca et al., 1999a; Gaspar-Escribano et al., 2004) and has been interpreted as the final stage of an aborted rift event responsible for the ENE motion of the Balearic promontory (Palano et al., 2015). Several normal active faults have been defined in the southwestern Valencia Trough thus far (Fig. 1): the Western Cabo Cullera Fault, Central–Western Cabo Cullera Fault, Central–Eastern Cabo Cullera Fault, Eastern Cabo Cullera Fault and Southwest Columbretes Fault (Perea, 2006). Some of these faults were previously recognised from vintage seismic lines (Diaz del Rio et al., 1986; Roca, 1992, 1996; Perea, 2006; Maillard & Mauffret, 2013), but fault traces and geometry were defined only very approximately. Similarly, the slip rates derived from the displacement of Plio-Quaternary seismic reflectors observed in the vintage seismic lines present high uncertainties (0.02 ±0.01 mm/yr; Perea, 2006). In the Valencia Trough, seismicity is characterised by low- to moderate-magnitude events (Fig. 1). The few available focal mechanisms (Stich et al., 2010; IGN, 2025) indicate a normal–oblique or strike slip kinematics, although these focal mechanisms present high uncertainties, mainly because they occur at long distances from seismic stations

and are registered with significant azimuthal gaps (González, 2017). According to the data published by the Spanish Earthquake Catalogue (IGN, 2025), this seismicity is very shallow, as most of the events are assigned depths of less than 10 km (Fig. 2). However, these data should be taken with caution, as the depths assigned to these earthquakes present high uncertainties (González, 2017).

In the onshore domain located west of the Valencia Trough, only one major active structure, namely, the Jumilla Fault, has been postulated (García-Mayordomo et al., 2012), together with other minor active faults (Alcoy, Mariola, and Benasau Faults). In this onshore area, several significant historical earthquakes have occurred, such as the 1396 Tavernes (I_{EMS98}=VIII-IX), 1620 Alcoy (I_{EMS98}=VIII-IX), 1644 Muro (I_{EMS98}=V) and 1748 Estubeny (I_{EMS98}=IX) earthquakes (Martínez Solares and Mezcua, 2002; IGN, 2025; Buforn et al., 2105; Buforn & Udías, 2022).

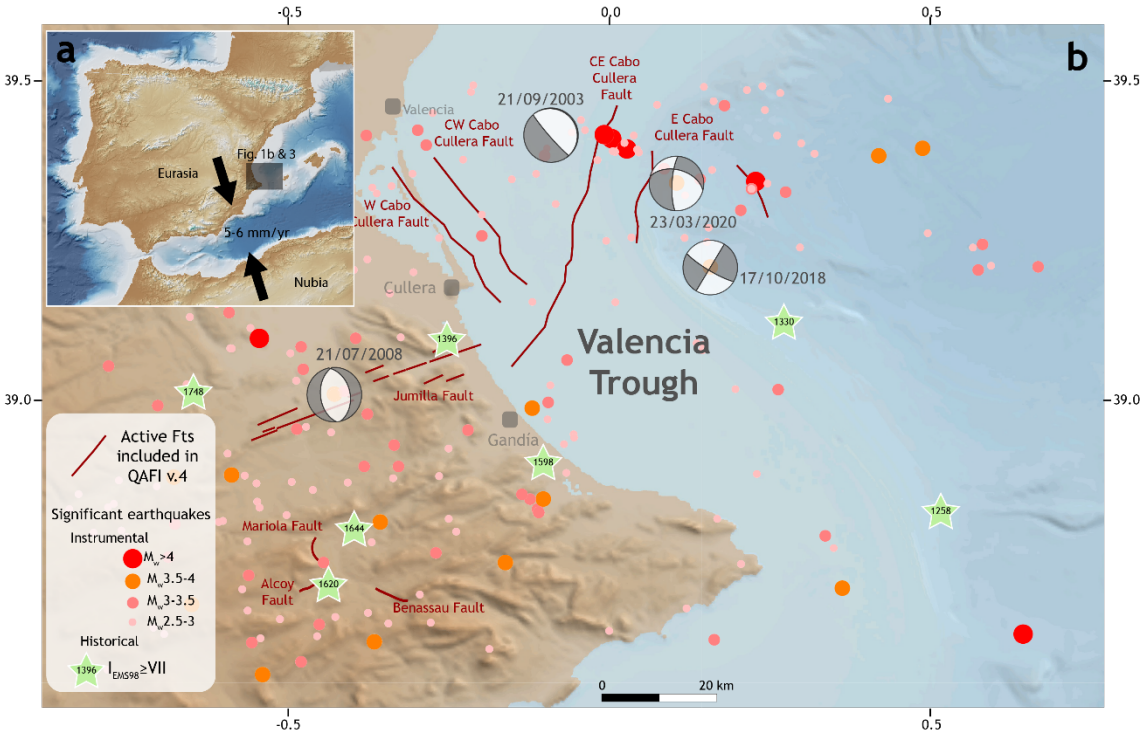

Fig. 1. a. Location of the Valencia Trough. Convergence vectors between Nubia and Eurasia are after DeMets et al., 1994; McClusky et al., 2003; Nocquet, 2012; Nocquet & Calais, 2003; Pérez-Peña et al., 2010; Serpelloni et al., 2007; Stich et al., 2006. b. Seismotectonic map of the southwestern Valencia Trough and surrounding

177 areas. Fault traces from Quaternary-Active Faults of Iberia database (García-
178 Mayordomo et al., 2012)

179

180

181

182 Fig 2. Seismicity of Mw>2.5 in the southwestern Valencia Trough shallower than 20
183 km since 1950 from the *Instituto Geográfico Nacional* database (IGN, 2025). a.
184 Distribution of the depth of seismicity. The horizontal axis represents distance along
185 the southwestern Valencia Trough in a SW-NE direction (from the SW shoreline to
186 the NE Mediterranean Sea). b. Energy (from magnitude) and depth histogram. In
187 both graphics events with 0 km of the assigned depth are not represented (fixed
188 depth).

3. Data

The interpretation of the offshore area is based on mainly 2D multichannel seismic reflection data calibrated with well data (Fig. 3). The central part of the study area is covered by a high-quality seismic survey acquired by Fugro-Geoteam with the RV Geo Baltic, processed by Robertson Research International Ltd. in 2002. The survey consists of 30 seismic sections with an average length of 90 km (totalling approximately 2,800 km). They are oriented WNW–ESE and NNE–SSW, with maximum spacings of 13 km and 6 km, respectively. The details regarding the acquisition and processing parameters can be found in Cameselle & Urgeles (2017). Most of the area affected by Plio-Quaternary faulting nearer to the coast is covered only by vintage 2D seismic lines from the late 1970s, acquired by various operators, which are publicly available upon request in the Instituto Geológico y Minero de España (IGME-CSIC) (http://info.igme.es/sigeof/). More than 100 of these seismic lines, with a total line length of approximately 2,500 km, were selected for mapping; although the quality of these lines varies from moderate to poor, the high-density grid spacing (varying from 1 to 3.5 km) allows fault mapping with reasonable confidence. The seismic interpretation was performed in two-way travel time (TWT) by using Move software (by Petex). The seismic dataset was converted to depths using velocity data derived from the Expanded Spread Profile (ESP) 7 (Pascal et al., 1992; Torné et al., 1992). A second-order polynomial trend was applied to establish time–depth relationships, ensuring strong correlation with the well data, similar to the methodologies of Fang et al. (2021).

The interpretation of seismic horizons is calibrated by 9 offshore petroleum exploration wells, all of which penetrate the entire Neogene section and whose bottoms are in Mesozoic rocks. Original well reports, log data (lithology, dipmeter, gamma–ray, sonic and resistivity data) and palaeontological data (from cuttings and sidewall cores) were retrieved from the IGME-CSIC archive (https://info.igme.es/hidrocarburos/). Well-to-seismic ties were established by integrating the sonic logs and using synthetic seismograms from end-of-well reports. Palaeontological analyses and range charts from the original well reports

were reviewed and adapted to the Mediterranean biozonation of Lirer et al. (2019) to obtain approximate absolute ages for the seismic horizons.

No seismic data were available for the onshore area of southern Valencia and only two deep exploration wells were drilled (Jaraco-1 and Perenchiza-1). However, stratigraphic information is available from 95 hydrogeological wells in the Valencia coastal plain, as are vertical electric sounding (VES) profiles acquired for hydrogeological surveys. The data are publicly available in the online IGME-CSIC databases IRYDA, BD Puntos Agua 2.0 and Sistema de Información Documental (SID) (accessible through https://info.igme.es/catalogo/).

In areas with poor seismic coverage, structural mapping was aided by regional Bouguer gravity anomalies processed with a Butterworth high-pass filter with a 1-degree cut-off frequency to highlight short-wavelength features of the data (by Getech, 2015).

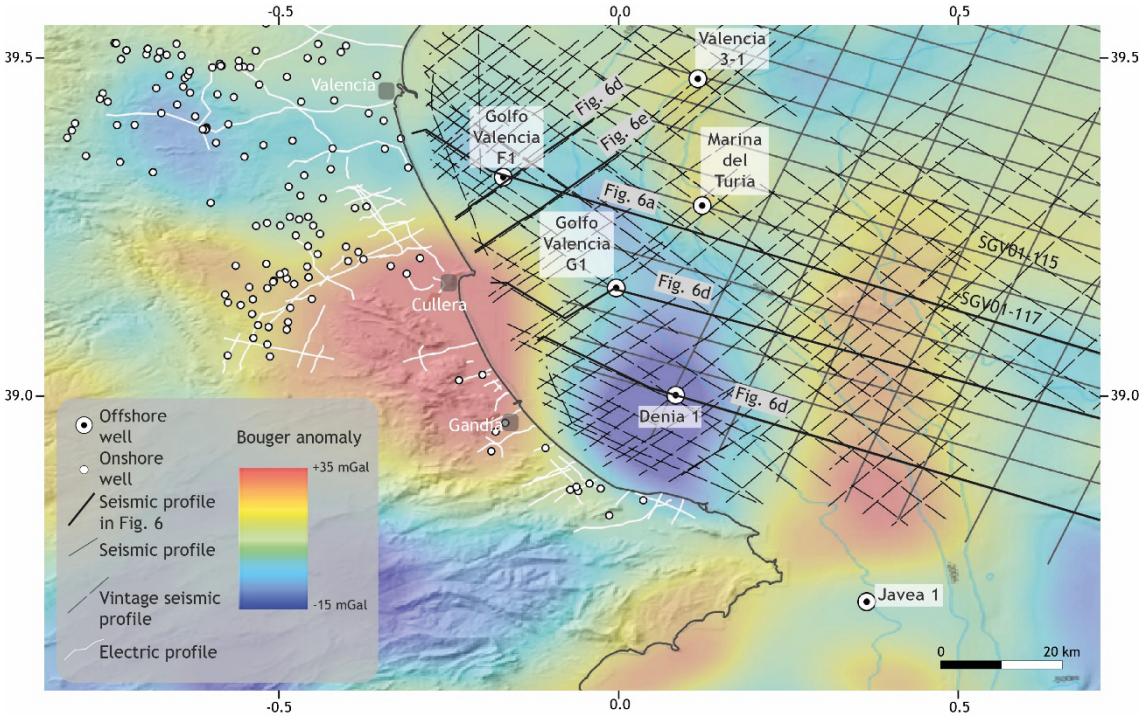

Fig. 3. Geophysical dataset used in this work. Filtered Bouguer anomaly data after Getech (2015). The location is shown in figure 1.

4. Stratigraphy

The general stratigraphic arrangement of the southwestern Valencia Trough (Fig. 4) consists of a rigid Palaeozoic–Middle Triassic basement overlain by a 1.5–7-km Upper Triassic–Quaternary stratigraphic cover. Here we present a new detailed stratigraphic framework for the late Miocene–Quaternary of the southern Valencia Trough. The definition of the pre-Neogene stratigraphic units presented in this work is based on mainly previous literature and our analysis of well data, as well as outcrops in the mainland for the most recent sediments.

The Upper Triassic succession (Fig. 4) consists of evaporites, shales and dolomites (Keuper Facies) (Vargas et al., 2009). The Upper Triassic deposits are overlain by Early Jurassic to Late Cretaceous carbonates and marls (Salas et al., 2001). erosive, angular unconformity that is directly overlain by Neogene deposits. The Cenozoic succession starts with a transition from continental clastic sediments to marine platform carbonates, ending with a deposit formed by progradational terrigenous shelf-talus sediments (Arche et al., 2010; Clavell and Berástegui, 1991; Etheve et al., 2018; Lanaja, 1987; Maillard et al., 1992; Ribó et al., 2016b, 2016a; Roca and Desegaulx, 1992; Soler et al., 1986). The Neogene succession onshore of the southwestern Valencia Trough (Fig. 4) mostly consists of middle–late Miocene continental to marginal marine deposits, including limestones, marls and coarse-grained detrital sediments. The top of the Miocene series is an erosional unconformity (Messinian Erosion Surface (MES) (Stampfli & Höcker, 1989; Lofi et al., 2011; Cameselle et al., 2014).

Pliocene–recent sediments form a large prograding shelf complex with prominent clinoforms visible in seismic data, which downlap onto the MES. Prominent undulations on slope foresets are visible on most seismic lines and are interpreted as sediment waves (Ribó et al., 2015). In the offshore wells, the stratigraphic succession consists of an overall shallowing-upward series of thick grey claystones with calcareous interbeds at the base, grading upwards into sandstones and shell beds at the top. No unconformities have been identified in the entire sequence, except for erosional gullies and canyons at the shelf edge. The Plio-Quaternary sequence reaches a maximum thickness of approximately 3000 m.

To determine the Plio-Quaternary depositional history and slip rate of major faults, six seismic horizons have been mapped and dated with palaeontological data from offshore wells, via the biostratigraphic scheme of Lirer et al. (2019). Starting from the Messinian unconformity at 5.3 Ma, seismic markers have been dated at 3.8 Ma (LO of *G. margaritae*), 3.3 Ma (FO *G. bononiensis*), 2.6 Ma (LCO *G. obliquus*) and 2.0 Ma (FO *G. truncatulinoides*). As no samples were collected from any of the offshore wells above the lower-middle Pleistocene interval, an additional marker (approximately 1.0 Ma) was picked halfway through the 2.0 Ma marker and seabed (0 Ma), assuming a constant sedimentation rate.

Isopach maps (Fig. 5) were produced for the intervals of Pliocene (MES to 2.6 Ma marker) and Pleistocene–recent (2.6 Ma marker to the seabed), revealing a significant shift in the location of the depocentre. The Pliocene depocentre is located very close to the southern coast near Denia, attaining a maximum thickness of approximately 1500 m, whereas the Pleistocene depocentre has prograded ca. 20 km to the NNW, reaching a thickness of more than 1750 m. The western shoreward edge of both the Pliocene and Pleistocene depocentres is controlled by very large NNW–SSE-trending normal faults (see below).

The described stratigraphic architecture indicates significant mechanical layering in the southwestern Valencia Trough. A rigid basement is overlain by a mechanically weak layer represented by the Upper Triassic Keuper Facies. Above this interval, a rigid Mesozoic carbonate succession is present, followed by a semirigid layer composed of primarily detrital deposits.

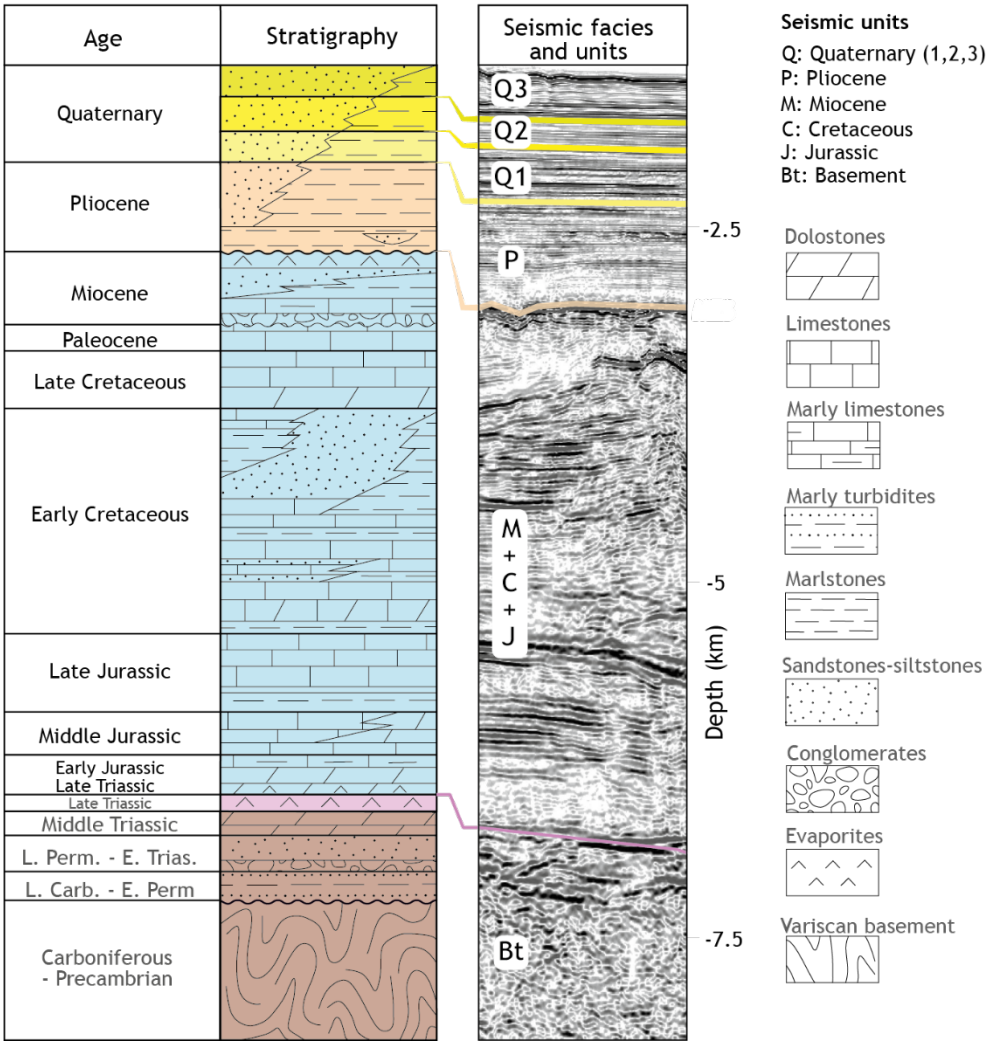

290

291 Figure 4: Chronostratigraphic diagram of the southwestern Valencia Trough.

292 Note that the depth scale shows maximum thicknesses of the units.

293

294

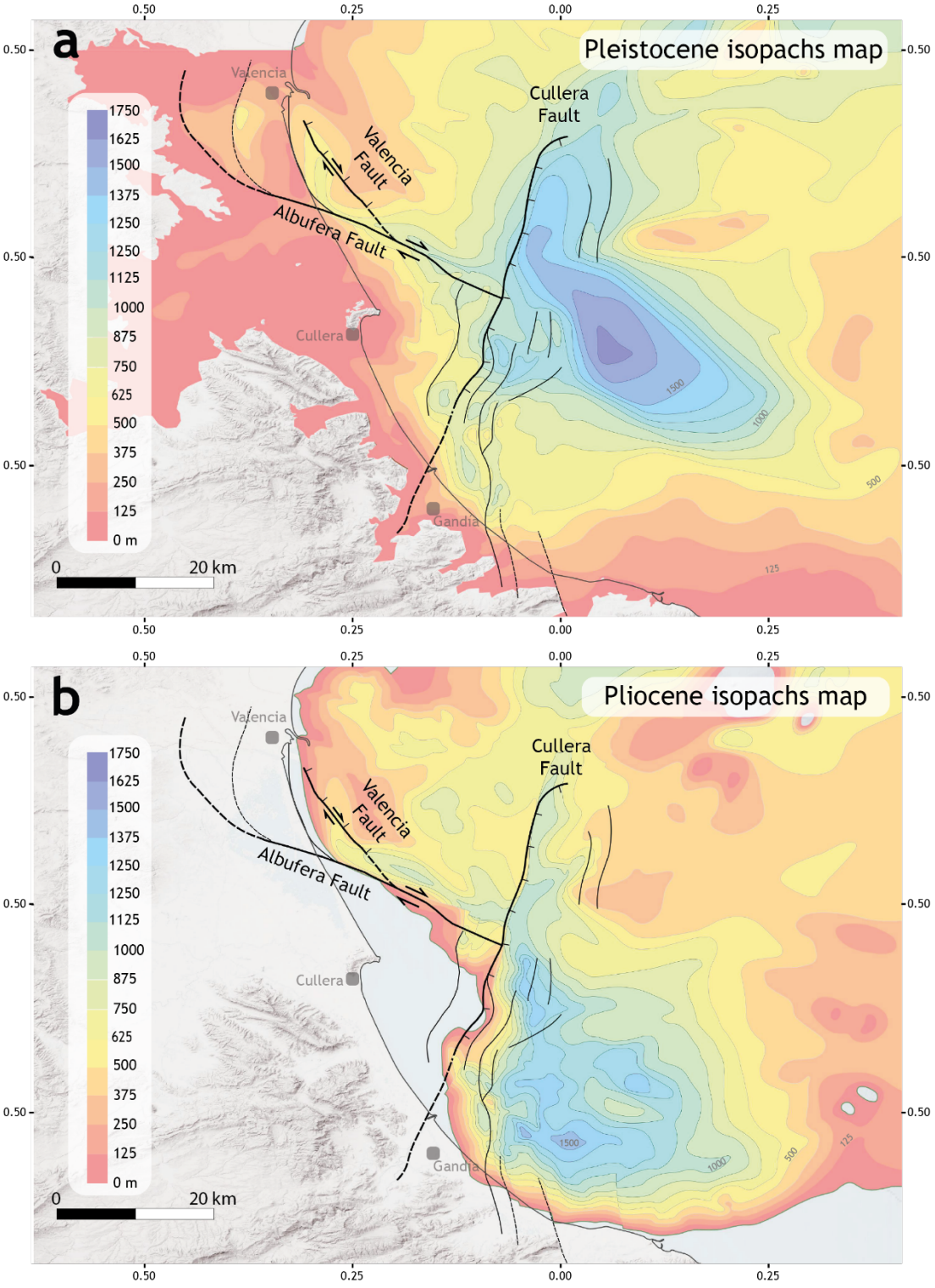

295

296 Figure 5. Isopach maps of the southwestern Valencia Trough for the Pleistocene (a)
297 and Pliocene (b). The traces of the active faults are also depicted. Fault traces

represent the horizontal projection of the direction line of the fault plane, located midway between the intersection line of the top-of-the-Pliocene horizon and the top-of-the-Quaternary horizon. Fault traces are derived primarily from their position on seismic profiles, supplemented by isopach maps and observed thickness variations in stratigraphic units, as indicated by the available wells. Dashed lines show interpreted traces. Modified from Ramos et al. (2025).

5. Main active faults in the southwestern Valencia Trough

In this section, we describe the main structural features of the southwestern Valencia Trough after the analysis of gravity data and isopach maps obtained from the subsurface dataset (seismic lines, wells and VES) (Figs. 3 and 5).

The filtered Bouguer anomaly map (Fig. 3) reveals a positive anomaly in the central part of the study area, referred to as the Cullera anomaly. This positive anomaly is surrounded by a region exhibiting a negative anomaly, particularly in the offshore area located east of Cullera. We interpret this pattern of anomalies to be because of mass excess associated with a basement high (Cullera positive anomaly) surrounded by a region with greater sedimentary cover (negative anomaly). This interpretation is further supported by the isopach maps derived from interpretation of the subsurface data (Fig. 5). The negative gravity anomaly correlates with an abrupt increase in the thickness of both the Pliocene and Quaternary sedimentary successions. Furthermore, the transitions in both the gravity anomaly and sedimentary thickness correspond to the positions of the main faults observed in the seismic dataset (see below). On the basis of this evidence, we propose that the southwestern Valencia Trough is structurally characterised by the presence of three major faults offsetting the basement and significantly influencing the stratigraphic evolution of the area. These three major faults are: the Cullera Fault, the Valencia Fault and the Albufera Fault (Fig. 5).

The structural configuration of the southwestern Valencia Trough is also influenced by the presence of Upper Triassic evaporites and shales at the base of the Mesozoic sedimentary cover. Major faults offsetting the Mesozoic–Quaternary succession present a listric geometry with a main ramp that flattens out in the Upper Triassic salt layer (Fig. 6). These geometries have been interpreted as evidence of a strain partitioning between the suprasalt and the subsalt successions (Etheve et al., 2016; Fang et al., 2021; Muñoz Martín & Vicente Muñoz, 1988). According to these interpretations, the Upper Triassic is a mechanically weak layer that induces tectonic decoupling within the seismogenic crust of the southwestern Valencia Trough. As a result, the deformation style of the suprasalt succession (cover) differs significantly from that of the subsalt succession (basement) (Etheve et al., 2018;

Fang et al., 2021; Ramos et al., 2023, 2025; Roma et al., 2018). The main difference is that normal faults present a listric geometry in the cover, while these faults are planar within the basement (see below).

The analysis of the seismic reflection profiles (Fig. 6) reveals three fault types: i) faults restricted to the subsalt basement; ii) faults restricted to the suprasalt cover; and iii) faults cutting through the sedimentary cover, basement and salt layer.

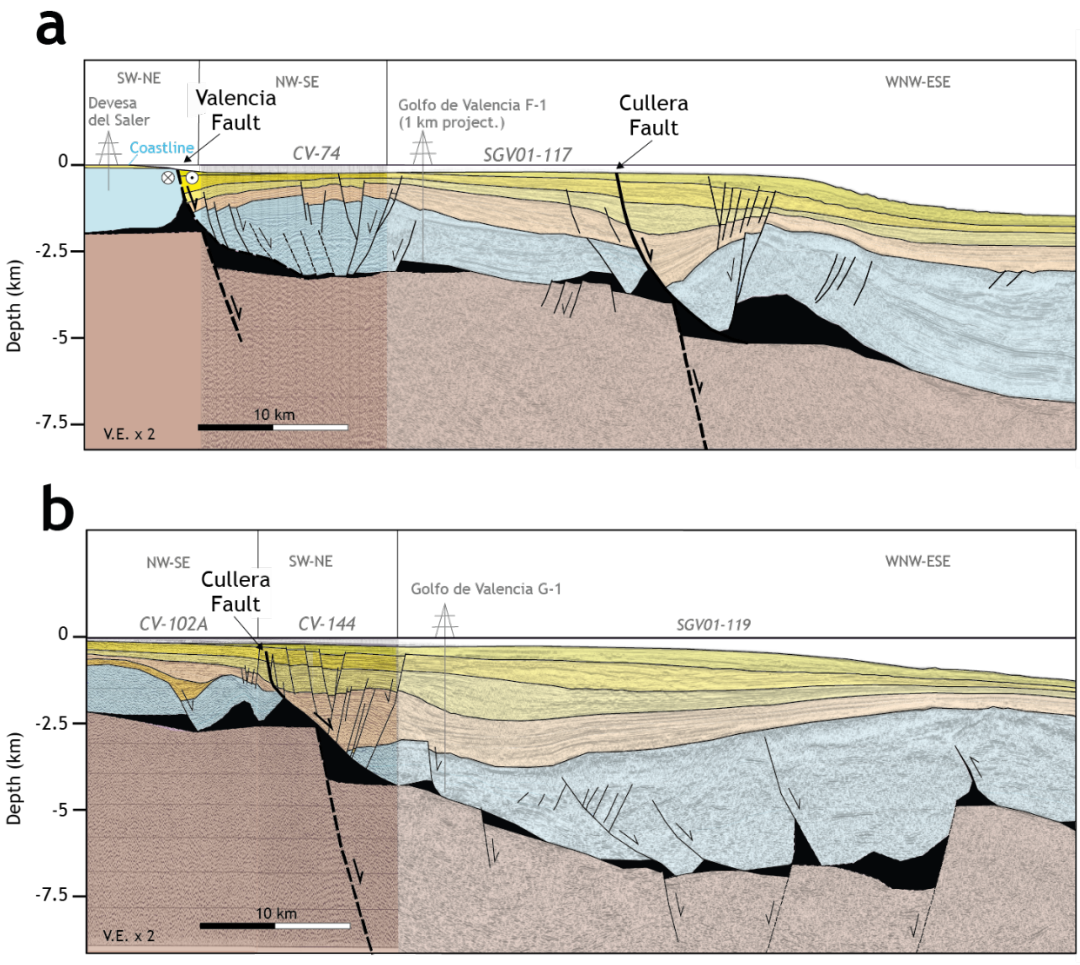

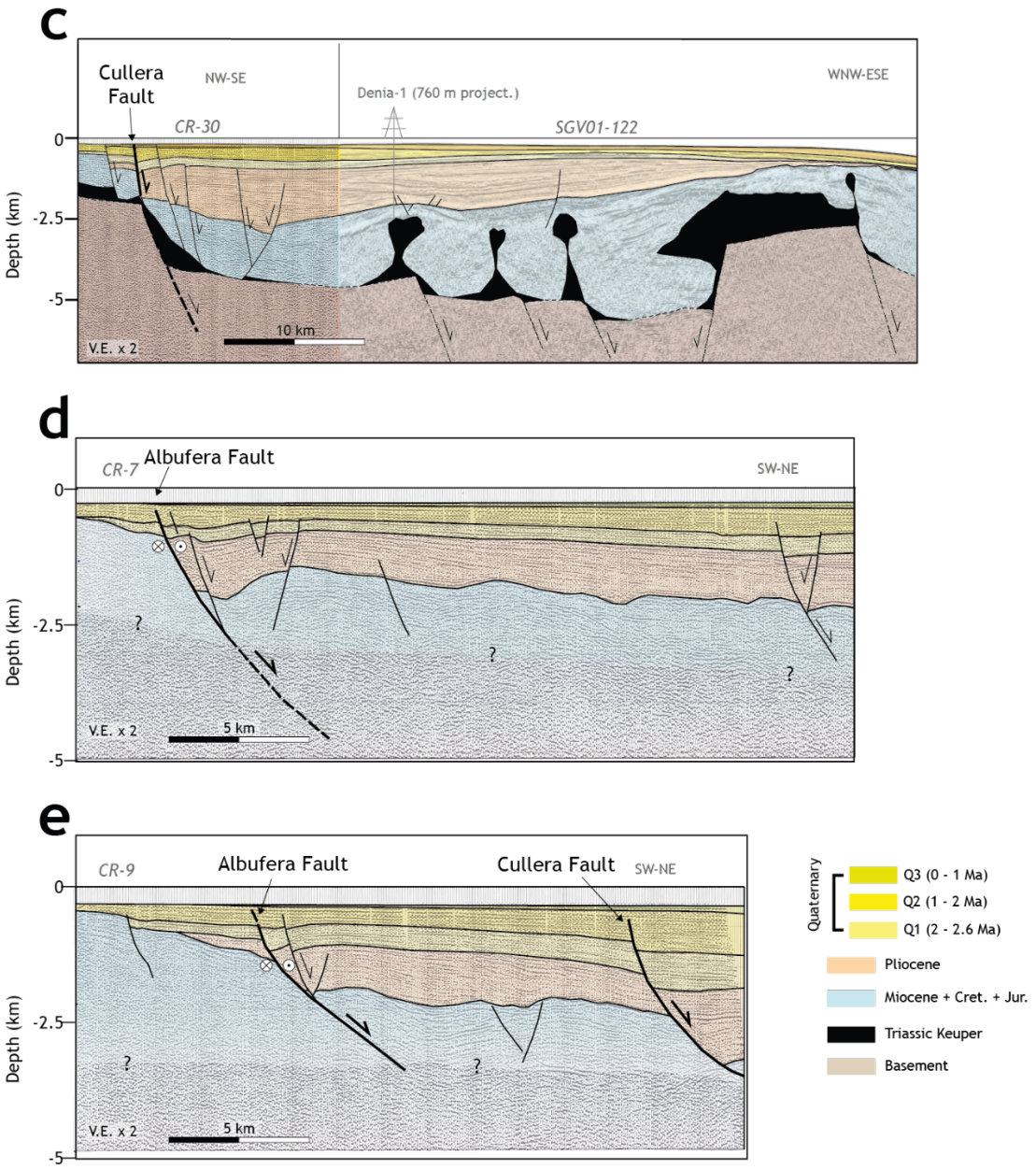

Fig. 6. Interpreted sections derived from onshore cross-sections (a) and the offshore 2D seismic profiles (a-e). Sections in a-d depict the structure of both the supra- and subsalt successions, while in sections in d-e only the suprasalt structure is represented. See Fig. 3 for the location. a-c sections after Ramos et al., 2025. Unit colours are as those in Fig. 4 (except for the Triassic unit). Note the x2 vertical exaggeration of all the sections.

5.1 Cullera Fault

The Cullera Fault is the longest along-strike fault in the region, spans approximately 59 km, and has the highest cumulative offset, with more than 1800 m of vertical displacement at the top of the Messinian horizon (Figs. 5 and 6).

The along-section geometry of the fault across the suprasalt succession is well imaged in the seismic reflection dataset (Fig. 6). The Cullera Fault is a normal, NNE–SSW-trending fault that dips highly towards the east. The fault offsets the entire suprasalt cover, including the 1 Ma horizon. Owing to the low resolution of the available bathymetric data, it is not possible to confirm whether the fault offsets the seafloor. The Cullera Fault displaces the top of the basement horizon, indicating that this fault involves both subsalt and suprasalt successions.

Within the basement, the Cullera Fault is poorly imaged in seismic profiles. Nevertheless, the available data suggest that it is a planar fault (Fig. 6). This is also supported by the absence of significant tilting of the basement-top horizon.

In contrast, the geometry of the Cullera Fault in the sedimentary cover is heterogeneous. In the northern area (Fig. 6), the part of the Cullera Fault offsetting the cover exhibits a listric geometry, which is responsible for the development of a rollover structure in the hanging wall (Fig. 6). Southwards, the listric geometry and related rollover fold becomes less pronounced (Fig. 6).

To better constrain the geometry of the Cullera Fault, we constructed a structural map of the fault by integrating fault traces identified in the seismic reflection dataset with isopach maps (Fig. 7). Additionally, a 3D model of the Cullera Fault, along with the two other major faults, was generated following a 2½D construction approach, integrating interpreted seismic profiles via interpolation. We employed the ordinary kriging algorithm implemented in MOVE software, a methodology consistent with previous approaches applied to analogous structures (Ramos et al., 2020Analysis of the reconstructed 3D fault indicates that the surface area of the Cullera Fault offsetting the sedimentary cover is approximately 360 km^2.

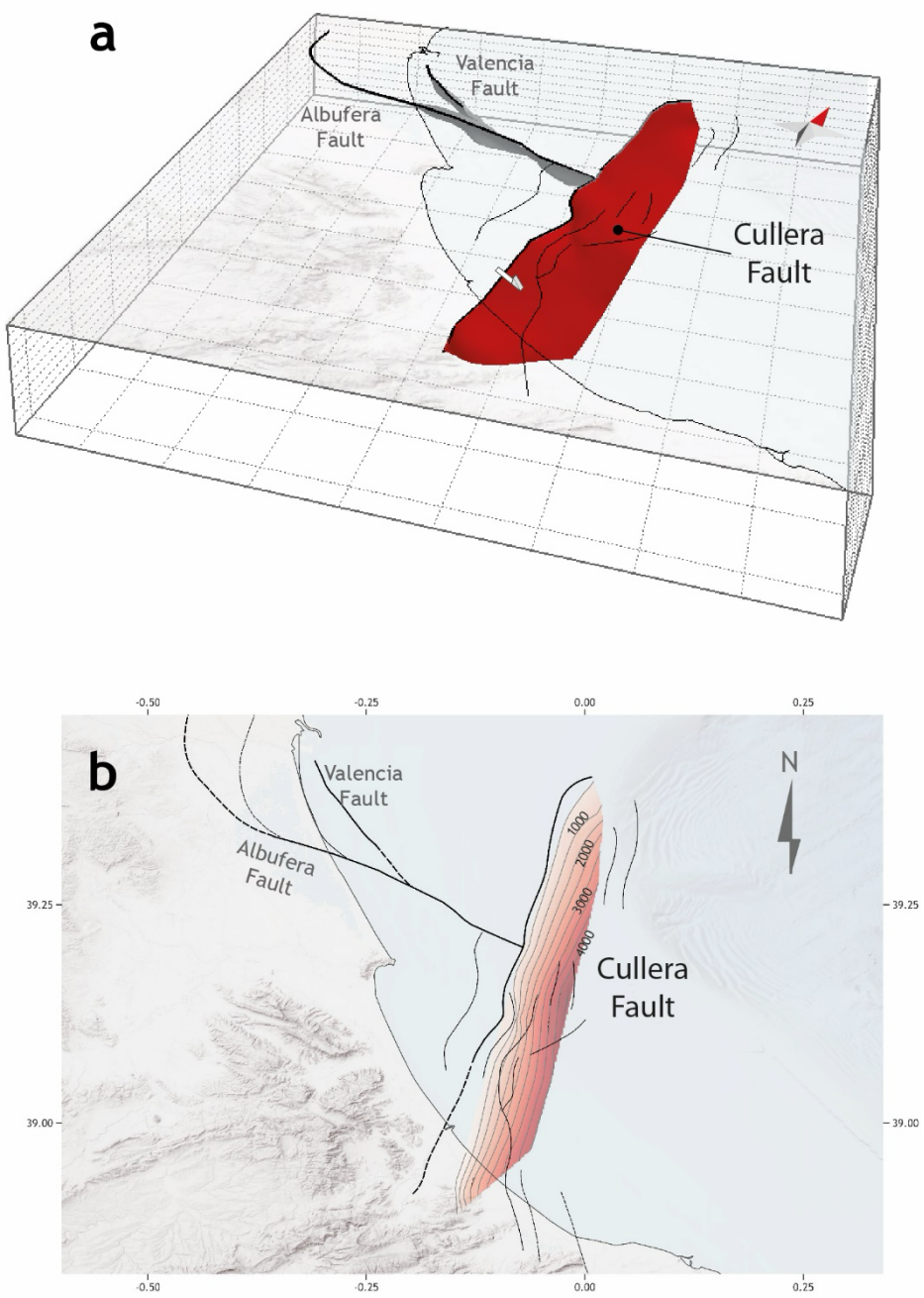

385

386 Figure 7. 3D model (a) and structural map (b) of the Cullera Fault (red surface).
387 Squares in figure 7a represent 10 km x 10 km. Note the red arrow pointing to the
388 north in figure 7a.

389

390 Several minor normal faults have developed in the hanging wall of the Cullera Fault
391 (Figs. 5). These faults displace only the suprasalt succession without affecting the
392 underlying subsalt units. In previous studies (e.g., Perea 2006; Roca 1992), distinct
393 names were assigned to these faults, such as the Western Cabo Cullera Fault,

Central Cabo Cullera Fault, and Eastern Cabo Cullera Fault. However, the improved resolution and quality of the new seismic dataset enable a more detailed characterisation of these tectonic structures, allowing for a reassessment of their nomenclature and role. We interpret these minor faults to be part of the damage zone associated with the main Cullera Fault.

The quality of the seismic dataset allows for an analysis of the slip rate of the Cullera Fault. This analysis is approximate, because of the resolution of the seismic profiles, the uncertainties in the recognition of the markers in the hanging wall and footwall, and the age of these markers. Net slip rates were obtained for the Top-Messinian, Top Pliocene, Top-Q1, and Top-Q2 horizons, with assigned ages of 5.3 Ma, 2.6 Ma, 2 Ma, and 1 Ma, respectively (Fig. 8). The slip rates for the Cullera Fault seem to have decreased over time, as the calculation yielded mean slip rates of 0.40 ± 0.1 mm/y for the Pliocene and 0.15± 0.1 mm/y for the Quaternary. This slip rate reduction could be the consequence of a change in the regional tectonic regime in the complex tectonic cadre of the western Mediterranean region. However, as the Cullera Fault is a salt-influenced structure, different mechanisms control fault offset. We discuss in section 6 the potential reasons behind this observed decrease in slip rate. In any case, we cannot dismiss that at least part of this apparent in-time evolution could be an artefact related to the epistemic uncertainties mentioned above.

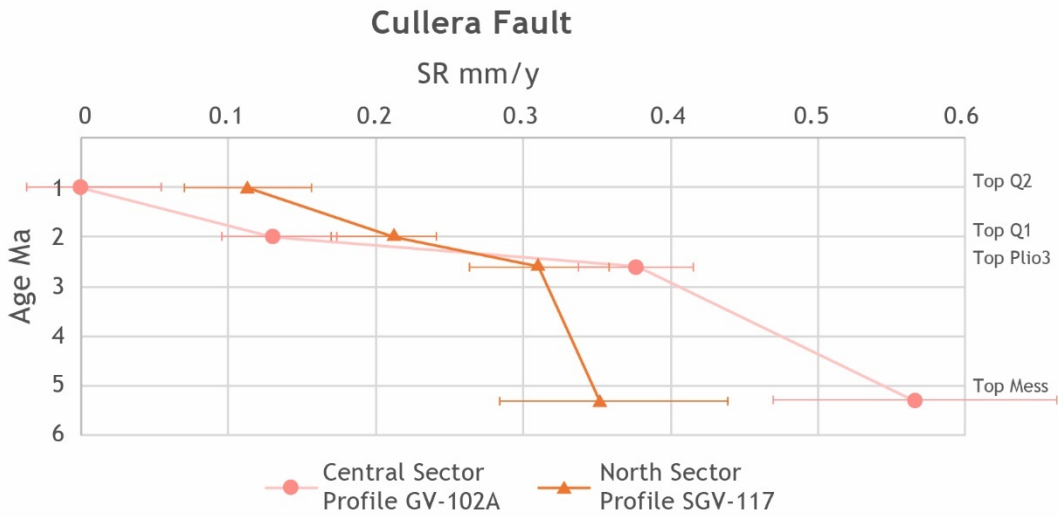

Figure 8. Long term slip rates (SR) for the Cullera Fault derived from the seismic profiles for the Top Messinian, Top Plio3, Top Q1, and Top Q2 horizons. The pink line and dots represent SR for the central sector of the fault. The orange line and triangles indicate SR for the north sector of the fault. The slip rates seem to decrease in time, from 0.40 ± 0.1 mm/y for the Pliocene to 0.15± 0.1 mm/y for the Quaternary. Error bars are estimated on the basis of uncertainties in the recognition of the markers and their ages.

5.2. Albufera Fault

The Albufera Fault (Figs. 5 and 6) is a newly defined active structure in the southwestern Valencia Trough. This NW–SE striking fault extends approximately 55 km and presents an oblique kinematic, with a major strike slip component and a minor normal displacement (see below). The Albufera Fault exhibits a maximum vertical offset of 1000 m for the Top-Messinian horizon. This would imply a long-term vertical slip rate of 0.2 ± 0.1 mm/y. The fault offsets both the supra- and subsalt successions (Figs. 5 and 6). The Albufera Fault is visible only in the vintage seismic reflection dataset, where it presents a low dip and a listric geometry.

The Albufera Fault appears to offset the entire suprasalt cover, including the 1 Ma horizon. As with other faults in the region, the low resolution of the available bathymetric data prevents us from determining whether this fault offsets the seabed. Nevertheless, high-resolution seismic profiles from the offshore shelf analysed by previous authors indicate seabed offsets caused by secondary normal faults likely associated with the Albufera Fault (Díaz de Río et al., 1986; Albarracín et al., 2013).

The available seismic dataset reveals a normal kinematic component for the Albufera Fault. However, mapping of small-scale fault traces in upper Pleistocene–recent sediments (interval between the seabed and the 1.8 Ma horizon) reveals that these faults are oblique to the main trend of the Albufera Fault, forming an en echelon pattern in map view, which suggests that the Plio-Quaternary reactivation of the main fault has a significant right-lateral strike-slip component. This dextral

component is consistent with the regional ENE–WSW direction of Plio-Quaternary extension in the southwestern Valencia Trough and kinematically consistent with NNW–SSE trending normal faults. The fault influences the Plio-Quaternary sedimentary infill of the southwestern Valencia Trough (Fig. 5). The isopach maps reveal that the Pliocene and Quaternary succession significantly increased in the hanging wall relative to the footwall. The listric geometry of the Albufera Fault is responsible for the development of a rollover anticline in the hanging wall (Fig. 6). This anticline is likely accentuated by the palaeoshelf edge of the late Tortonian–early Messinian shelf, which is located in the central part of the rollover structure. To further constrain the geometry of the Albufera Fault, a structural map and a 3D model of the fault was constructed (Fig. 9). Analysis of the reconstructed 3D fault surface indicates that the fault encompasses an area of approximately 560 km^2.

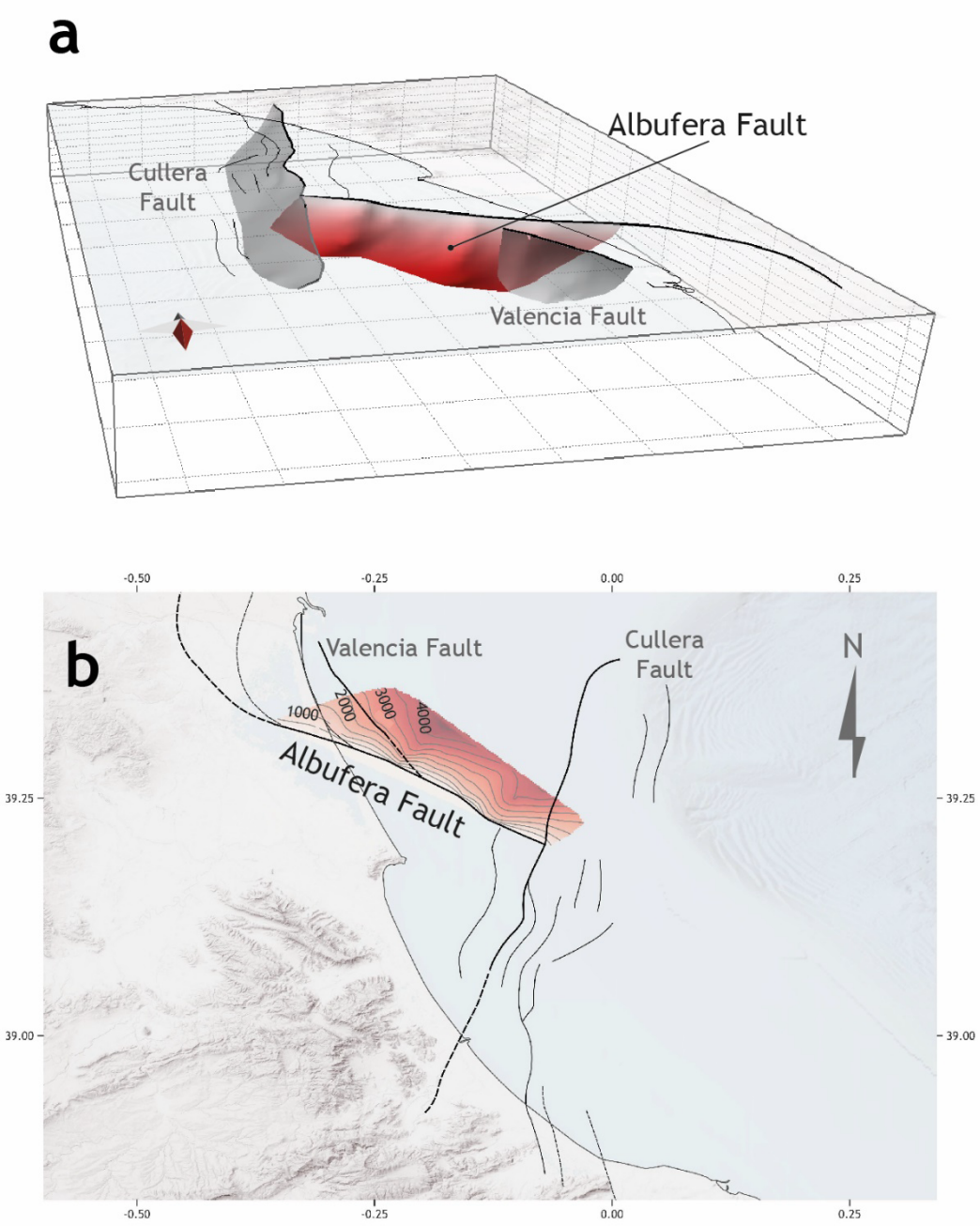

457

458

459

460

461

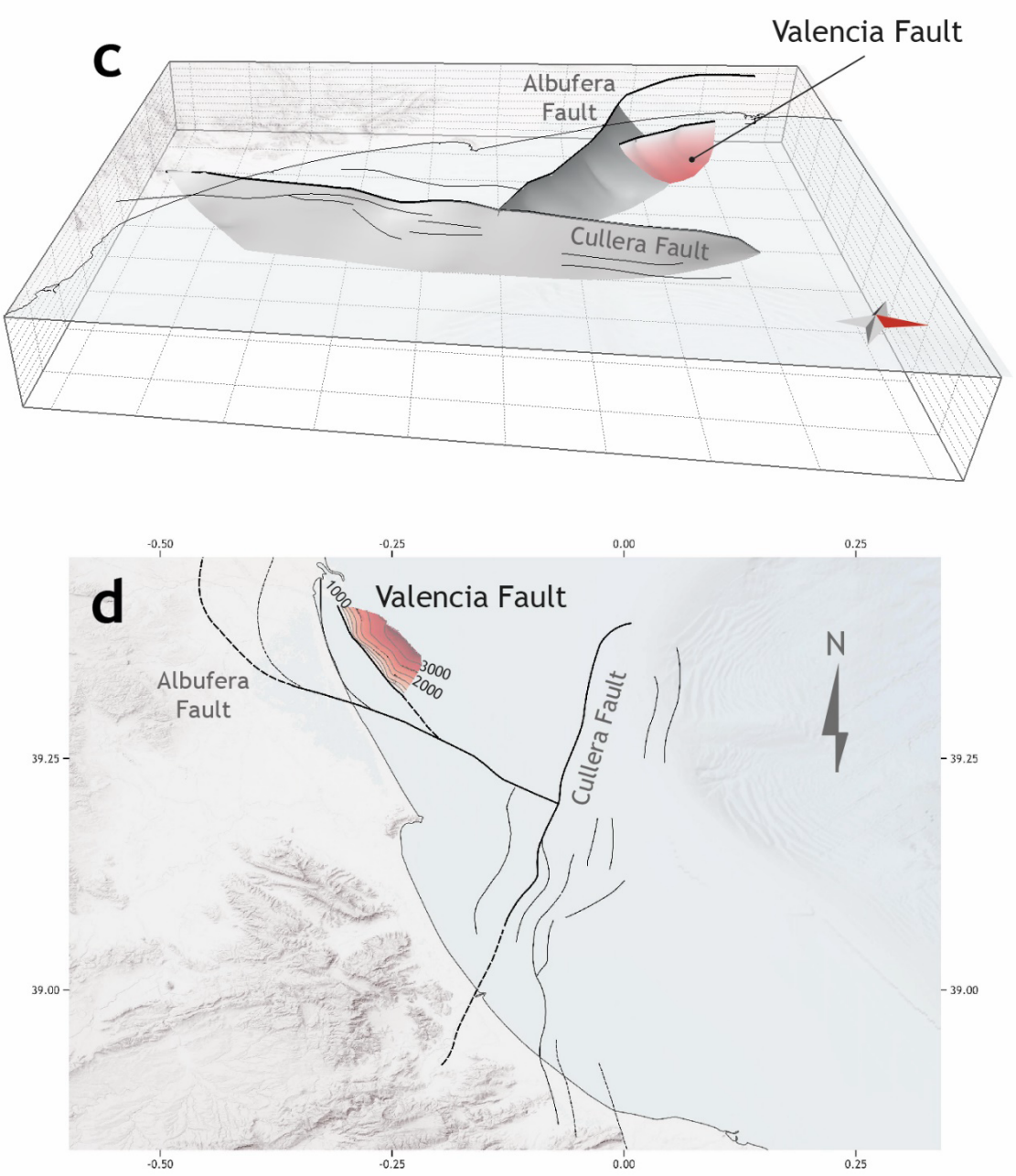

462

463 Figure 9. 3D model and structural map of the Albufera Fault (a and b) and the
464 Valencia Fault (c and d). Squares in the 3D models represent 10 km x 10 km boxes.
465 Note the red arrow pointing to the north in figures 9a and 9c.

466

467

468 **5.3 Valencia Fault**

In this section, we describe the Valencia Fault (Figs. 5 and 6). This structure could correspond to the Western Cabo Cullera Fault (sensu Perea, 2006). The Valencia Fault presents a length of approximately 20 km and has a significant impact on the distribution of Quaternary depocentres. The Valencia Fault present a normal component, as it vertically displaces both the supra- and subsalt successions (see below) (Figs. 5 and 6). However, taking into account the general structural arrangement of the southwestern Valencia Trough, we postulate that the Valencia Fault presents also a strike-slip component.

This NNW–SSE trending, steeply dipping fault is imaged primarily in the vintage seismic reflection dataset, where it exhibits a listric geometry, at least in the portion offsetting the suprasalt succession (Fig. 6). The Valencia Fault vertically offsets the entire suprasalt cover, including the 1 Ma horizon. However, owing to the low resolution of the available bathymetric data, it is not possible to determine whether this fault offsets the seabed. The Valencia Fault also displaces vertically the top of the basement horizon, indicating that this structure involves both subsalt and suprasalt successions. Within the basement, the Valencia Fault is not well-imaged in the seismic profiles, but the absence of tilting in the basement-top horizon suggests that it is a planar fault (Fig. 6). The Valencia Fault and its secondary strands very likely continue onshore below the City of Valencia. The lack of onshore seismic data hampers the mapping of these fault strands, but their presence can be inferred from the abrupt Plio-Quaternary thickness changes observed in water wells and vertical electric sounding profiles.

To further constrain the geometry of the Valencia Fault, a structural map and a 3D model of the fault was constructed (Fig. 9). Analysis of the reconstructed 3D fault surface indicates that the fault encompasses an area of approximately 208 km^2.

6. Evolutionary growth of the Cullera Fault: interplay between tectonics and salt withdrawal.

This section aims to provide further insights into the evolution of the active faults in the southwestern Valencia Trough. The low resolution of the vintage seismic dataset limits the ability to perform a detailed analysis only for the Cullera Fault. To analyse recent along-dip variations in throw, we constructed throw-depth plots (T-z plots) for the post-Messinian markers (Fig. 10). These plots provide insights into the evolutionary growth of the fault (Mansfield and Cartwright, 1996; Hongxing and Anderson, 2007). The quality of the available seismic reflection dataset allows this analysis to be performed on two seismic profiles located in the northern part of the fault, where the listric geometry is well-developed (LINES SGV01-115 and SGV01-117; Figs. 3 and 6).

We computed T-z plots for six suprasalt horizons: Top-Messinian, Top Plio1, Top Plio2, Top Plio3, Top Q1, and Top Q2 (Fig. 10). The T-z plots for the Cullera Fault reveal a general increase in the throw and throw gradient with depth. We postulate that the increase observed in the throw is the result the differing ages of the horizons, older horizons show greater offset because they have been displaced over a longer time interval. As regards throw gradients, the data indicate two distinct portions: (i) the lower portion, with higher throw gradients, includes horizons from the Top Messinian to the Top Pliocene; (ii) the upper portion, with lower throw gradients, comprises the Quaternary horizons. This distinction is particularly pronounced in the southern seismic line (line SGV01-117, Fig. 6). Here, the throw gradient decreases, from 2.38–2.98 in the lower portion to 0.22–0.10 in the upper portion.

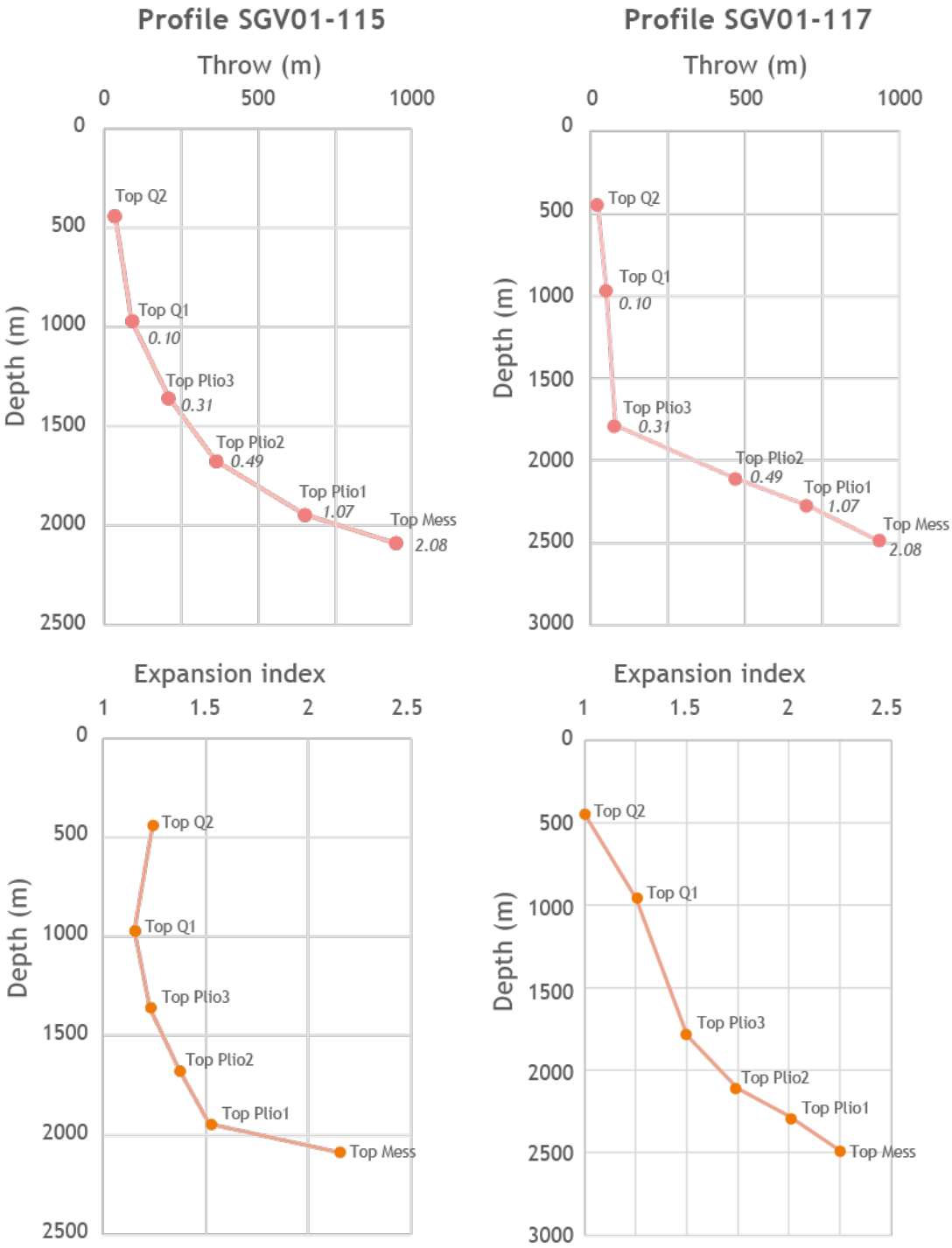

Figure 10. Throw depth (T-z) and expansion index plots for the Cullera Fault computed from profiles SGV01-115 and SGV01-117. The numbers within the T-z plots indicate the throw gradient for the corresponding interval. The T-z plots reveal an increase in the throw and throw gradient, with a higher throw gradient for the Top Messinian–Top Pliocene interval and a lower throw gradient for the Quaternary interval.

525 The Cullera Fault significantly influences the Plio-Quaternary sedimentary infill of
526 the southwestern Valencia Trough. Isopach maps indicate a marked increase in the
527 thickness of both Pliocene and Quaternary successions in the hanging wall with
528 respect to the footwall (Fig. 5). To quantify this relationship, we computed the
529 expansion index (Thorsen, 1963; Rouby et al., 2003; Jackson and Rotevatn, 2013) for
530 the post-Messinian stratigraphic units (Fig. 10). The expansion index consistently
531 exceeds 1 across all the analysed intervals, indicating a synkinematic deposition in
532 these units. The Pliocene units exhibit a greater expansion index than the
533 Quaternary units do, with the difference being particularly pronounced in the
534 southern seismic line (Fig. 6 LINE SGV01-117).

535 Finally, to shed light on the mechanisms controlling the creation of accommodation
536 space related to the Cullera Fault, we analyse the tectonic–stratigraphic
537 arrangement of the hanging wall units. To discuss this point, we compare the
538 geometries observed in the southwestern Valencia Trough with analogous
539 stratigraphic geometries in the Danish North Sea, where they have been interpreted
540 in terms of the evolution of salt-influenced faults (Duffy et al., 2023 and references
541 therein). In such a setting, two mechanisms create accommodation space: fault
542 displacement and load-driven salt withdrawal in the hanging-wall. These two
543 mechanisms can act separately or contemporaneously in time. When the
544 accommodation space generated by the fault offset exceeds that created by salt
545 withdrawal, the depocentre axis remains adjacent to the fault. In contrast, when
546 salt-related accommodation space is dominant, the depocentre migrates away
547 from the fault (Duffy et al., 2023).

548 In the northern part of the Cullera Fault, where the rollover structure is well
549 developed (Fig. 6), the position of the Plio-Quaternary depocentre in the hanging-
550 wall varies along the dip direction. The Pliocene depocentre remains in the
551 immediate hanging wall of the fault. Therefore, we interpret that, during the
552 Pliocene, the accommodation space generated by the displacement of the Cullera
553 Fault exceeded that produced by the accommodation space related to salt
554 withdrawal. During the deposition of unit Q1, the depocentre migrated basinwards,
555 suggesting that salt withdrawal-related accommodation space outpaced that

related to fault displacement. Finally, during Q2 and Q3, the depocentre axis shifted towards the fault, indicating that fault displacement-related accommodation space regained dominance over salt mobility. We postulate that this evolution in the location of depocentres is related to the mechanisms responsible for the creation of accommodation space.

All the above-described features shed light on the evolution of the salt-influenced Cullera Fault. As previously discussed, the creation of accommodation space results from two mechanisms: tectonic offset along the fault and displacement related to salt withdrawal. Both mechanisms act cumulatively; that is, both mechanisms produce slip along the Cullera Fault and create accommodation space. The migration of successive depocentres suggests that, during the Pliocene, accommodation space related to tectonic offset was greater than that created by salt withdrawal. As the throw gradient is high (≈ 2.4) during this period, we postulate that both mechanisms were active. During the deposition of Q1 (2.6–2 Ma), the position of the depocentre suggests that salt mobility became the dominant mechanism, likely due to a decrease in fault activity, an increase in salt withdrawal, or both. As throw gradient decreases during this period, we postulate that a decrease in the fault displacement rate could be the reason for the change in the main mechanism. Finally, during the rest of the Quaternary (2 Ma to present), fault displacement-related accommodation space once again exceeded that created by salt withdrawal. The constant throw gradient observed during this period with respect to the previous time interval (2.6–2 Ma) suggests that the change in the main mechanism was due to a reduction in or cessation of salt withdrawal. This interpretation is further supported by the off-fault geometry of the Q2–Q3 sedimentary bodies, as no significant change in thickness is observed above the salt withdrawal-related anticlinal crest located east of the Cullera Fault (Fig. 6).

Therefore, according to the above exposed, we postulate that, during the Pliocene and lower Quaternary (up to 2 Ma ago), the offset of the Cullera Fault was produced by both tectonics and salt withdrawal, being the first mechanism dominant during the Pliocene and the second during the 2.6–2 Ma time span. From that moment to the present salt withdrawal ceases (or significantly reduces), and tectonics

becomes the only (or very dominant) process. The reduction of salt movement is possibly due to the complete withdrawal of mobile salt and the formation of a weld below the hanging wall. This evolution could also explain the slip rate decreases observed for the Cullera Fault (Fig. 8). A higher slip rate is expected during the Pliocene, when both tectonics and salt withdrawal were active. Once salt withdrawal ceases or significantly decreases, a corresponding decrease in the slip rate is also expected.

7. Influence of mechanical layering on the seismic potential: the case of the southwestern Valencia Trough

The southwestern Valencia Trough has a distinct mechanical stratigraphy characterised by three layers: a subsalt basement, a weak mechanical layer composed of Triassic evaporites, and overlain Mesozoic–Quaternary sedimentary succession. Triassic evaporites are well documented for their ductile behaviour, which enables them to act as regional detachment layers (e.g., Morley et al., 2003; Jackson and Hudec, 2005) and inhibits the propagation of faults (e.g., Withjack et al., 1990; Pascoe et al., 1999; Maurin and Niviere, 2000; Withjack and Callaway, 2000; Richardson et al., 2005; Ford et al., 2007; Kane et al., 2010; Marsh et al., 2010). Moreover, mechanically weak layers have been shown to induce full or partial geometric and kinematic decoupling between sub- and supradetachment successions (e.g., Stewart et al., 1997; Withjack and Callaway, 2000; Ford et al., 2007; Tvedt et al. 2013). In this section, we focus on the implications of this mechanical arrangement in terms of how the presence of a weak mechanical layer influence the vertical propagation of seismic ruptures.

In an active region, tectonics are generally the main driving mechanism of fault displacement. However, in the case of salt-influenced faults, displacement can also result from salt withdrawal. Our analysis of the evolution of the Cullera Fault presented in the previous section indicates that the fault offset is related to the interplay between two mechanisms: tectonic offset along the fault and displacement related to salt withdrawal. Our analysis also reveals how these two processes interact with each other. Consequently, in areas with salt-influenced faults, seismicity can potentially be produced from either mechanism or a combination of both.

In terms of seismic potential, there is a significant difference between a tectonic earthquake and a salt-withdrawal earthquake. This difference lies in the maximum potential thickness of the seismogenic layer involved in the rupture. Tectonic stress affects the entire crust; therefore, strain related to tectonic accumulates both in the suprasalt and subsalt successions. Consequently, a tectonically driven earthquake could theoretically rupture the entire seismogenic crust. In contrast, a salt

withdrawal-related earthquake would imply offset restricted to the suprasalt succession, as in this case displacement surface coalesces into the salt layer. Therefore, in an earthquake restricted to the suprasalt succession, the thickness of the seismogenic layer is limited by the depth of the mechanically weak layer, reducing the maximum potential rupture area and, consequently, the seismic potential. A salt-withdrawal-related earthquake could induce a vertical stress drop related to salt displacement, potentially triggering displacement in the subsalt succession and leading to a complex rupture. Similarly, a tectonically driven earthquake may rupture only the suprasalt succession.

Despite the mechanism driving seismicity, the presence of a weak mechanical layer within the seismogenic crust significantly influences the seismogenic potential of active faults. We hypothesise that this weak layer could locally hinder the effective vertical propagation of a rupture, thereby resulting in faults being seismogenically bounded. Specifically, the total or partial decoupling induced by the weak evaporitic layer may limit the effective width of the seismogenic layer. This hypothesis is independent of the weak layer composition; therefore, our hypothesis can be extended to any region with a similar structural configuration.

Significant earthquakes (Mw > 6) typically nucleate at depths greater than 5 km. However, recent events in central Italy and France have demonstrated that very shallow (2–5 km) earthquakes of moderate magnitude (Mw 5–6) can also occur (Chiaraluce et al., 2017; Godano et al., 2025; Improta et al., 2019). In the southwestern Valencia Trough, the thickness of the supra-salt succession is slightly less than 5 km. Therefore, while the probability of a significant earthquake nucleating within the supra-salt succession is low, it is not zero. In this section we evaluate the seismic potential of these (unlikely) supra-salt ruptures. The case of central Italy could be taken as a geologic and tectonic analogous of the southwestern Valencia Trough. Central Italy resembles the southwestern Valencia Trough as both regions are presently dominated by extensional tectonics, and both are characterised by a pronounced mechanical layering in the upper crust. Recently, central Italy has undergone high seismicity, including the 1997-1998 Umbria-Marche, 2009 L'Aquila, and 2016-2017 Amatrice-Norcia seismic sequences

(Chiaraluce et al., 2003; Valoroso et al., 2013Chiaraluce et al., 2017; Improta et al., 2019; Michele et al., 2020). The area of central Italy where these seismic sequences took place is characterized by a complex geological framework consisting of several geological domains. Most of this area belongs to the Umbria-Marche fold-and-thrust belt. This belt consists of a crystalline basement overlain by a 3-8-km-thick Mesozoic–Quaternary sedimentary cover (Menichetti and Coccioni, 2013). The sedimentary Mesozoic succession starts with a 1.2 km thick salt layer (Anidriti di Burano Formation; Martinis and Pieri, 1964) acting as a mechanical weak layer. That is, similar to the southwestern Valencia Trough, the seismogenic crust of central Italy is characterised by the presence of a mechanically weak layer. As a consequence of thrusting during the Miocene-Pliocene, this weak layer is vertically repeated in some sectors (Barchi et al., 2021). Therefore, in central Italy the seismogenic crust includes from one to three weak layers.

Central Italy undergoes extension responsible for normal active faults. These active normal faults are the seismogenic sources of the seismic sequences occurred in the last decades (e.g., Boncio et al., 2004; Barchi and Mirabella, 2009), as well as several historical events (Rovida et al., 2020). Normal active faults in central Italy present a listric geometry in the sedimentary cover and offset the top of the basement (Barchi et al., 2021). The 1997-1998 Umbria- Marche and 2016-2017 Amatrice-Norcia seismic sequences nucleated within the suprasalt succession, including main events (Mw 5-6) with very shallow centroids (3-4 km; Barchi et al., 2021).

Based on the tectonic and stratigraphic similarities above exposed, we propose that the southwestern Valencia Trough may exhibit a comparable pattern of seismicity to that of central Italy. Specifically, we hypothesise that seismic events in the southwestern Valencia Trough could also have nucleated within the suprasalt succession and in the basement. Furthermore, we postulate that large earthquakes in the southwestern Valencia Trough could also rupture both mechanical layers. Available centroid data for the southwestern Valencia Trough suggest that most earthquakes nucleate at depths between 1 and 13 km (Fig. 2). Although these depth estimates carry significant uncertainties, we interpret this dataset as supporting

687 evidence for our hypothesis that seismicity in the southwestern Valencia Trough
688 nucleates both in the basement and in the cover.

689 From this hypothesis we evaluate the seismic potential of these (unlikely) supra-salt
690 ruptures. A widely used approach to characterise the seismic potential of an active
691 fault involves earthquake fault scaling relationships. These relationships estimate
692 the seismic parameters of an active fault based on its geometric and/or kinematic
693 features (Kanamori and Anderson, 1975; Geller, 1976; Wells and Coppersmith;
694 1994; Stirling et al., 2002 and 2013; Leonard, 2010 and 2014; among many others).
695 In the case of the southwestern Valencia Trough faults, the available data support
696 characterisation on the basis of geometric features, such as fault area, length, or
697 width. However, the mechanical layering observed in the southwestern Valencia
698 Trough necessitates the cautious application of these scaling relationships. The
699 influence of the weak mechanical layer introduces complexities that may not be
700 fully accounted for by traditional scaling methods.

701 As we mentioned previously, most empirical source-scaling relationships for crustal
702 earthquakes correlate the moment magnitude (Mw) with the fault dimensions
703 (length, width, and/or area; Kanamori and Anderson, 1975; Geller, 1976; Wells and
704 Coppersmith; 1994; Stirling et al., 2022; Leonard, 2010; among many others). We
705 propose that when these scaling relationships are applied to regions with a weak
706 mechanical layer, the role of this layer should be explicitly considered in the
707 analysis. This is because the presence of a weak layer can potentially hinder the
708 effective vertical propagation of a rupture, thereby limiting the effective width of the
709 seismogenic layer. This consideration is particularly relevant for earthquakes that
710 nucleate above the weak layer. We propose including a correction factor in the
711 empirical relationships that explicitly accounts for cases where earthquakes are
712 more likely to involve only part of the seismogenic layer due to mechanical
713 heterogeneities within the crust. This factor would aim to provide a more accurate
714 seismic characterization of faults in regions with such a structural arrangement.

715 Several studies suggest that the downdip width of the seismogenic crust (the
716 thickness of seismogenic crust measured along the fault plane) can constrain the
717 maximum magnitudes of earthquakes (Hyndman, 2007; Ruff and Kanamori, 1983;

718 Weng & Yang, 2017). For large-magnitude events involving the entire seismogenic
719 crust, some scaling relationships account for the constraint on fault-width rupture
720 growth relative to fault-length rupture growth by incorporating a change in slope in
721 width-to-length scaling (Leonard, 2010; Yen and Ma, 2011; Leonard, 2014; Cheng et
722 al., 2019; Huang et al., 2024). This change in slope reflects the width of the
723 seismogenic crust, which imposes a limit on rupture propagation owing to
724 variations in the mechanical behaviour of the crust. We propose a similar approach
725 to evaluate the seismic potential of regions characterised by a weak mechanical
726 layer within the upper crust, such as the southwestern Valencia Trough.

727 Our approach involves including the rupture aspect ratio when calculating the
728 geometric parameters of an active fault. Specifically, we propose that, instead of
729 using the total area or length of the fault as direct inputs to scaling relationships, a
730 correction factor should be applied to these geometric parameters. This correction
731 factor is based on the empirical aspect ratio of faults. For example, consider an
732 earthquake nucleating above a weak mechanical layer. Two potential scenarios for
733 the propagation of such an earthquake can be envisioned: i) that it propagates
734 through the basement–cover interface or ii) that it remains restricted to the
735 succession above the weak layer. In the first scenario, the potential maximum
736 rupture area can be calculated by multiplying the fault length by the fault width. Any
737 area-based or length-based scaling relationship can then be applied. This scenario
738 represents the maximum seismic potential of the fault.

739 In the second scenario, where rupture propagation is restricted to succession above
740 the weak layer, a simplistic calculation of the fault area would multiply the total fault
741 length by the thickness of the ruptured succession (Fig 11). However, since the
742 hypothesised rupture offsets only the succession above the mechanically weak
743 layer, the width of the rupture is significantly limited. This would result in a highly
744 elongated rupture with an unusually high aspect ratio, deviating from commonly
745 observed values (Nicol et al., 1996; Stock & Smith, 2000). For this second scenario,
746 we propose using the thickness of the ruptured succession as a limiting factor.
747 Specifically, the rupture area should be calculated by multiplying the width of the
748 fault (based on the thickness of the succession above the weak layer and corrected

by the fault dip) by the total fault length weighted by the aspect ratio (Fig 11). This weighted area can then be used as input in any area-based scaling relationship. We consider that this calculation offers a more realistic estimation of the maximum seismogenic potential for events rupturing only the succession above the weak layer. Finally, we recommend avoiding length-based scaling relations for this second scenario, as such relations implicitly assume a rupture of the entire seismogenic crust.

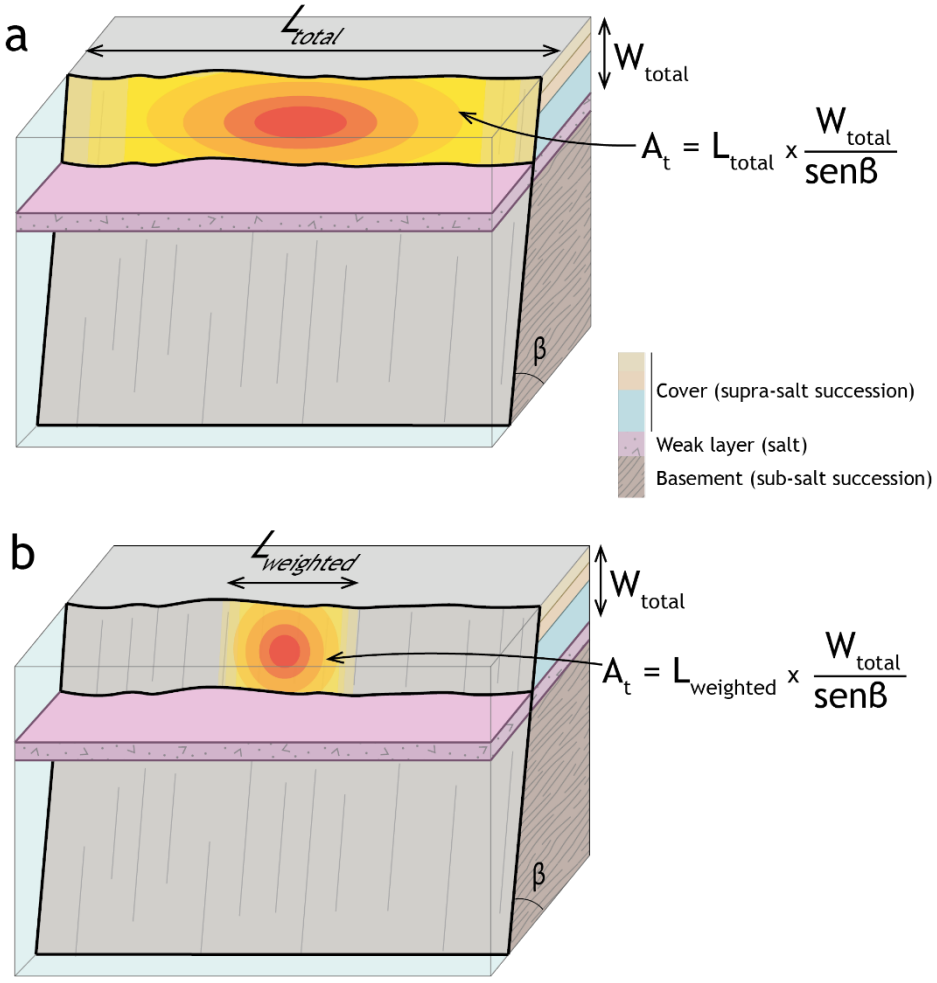

Figure 11. Conceptual model of the weighted rupture area of an earthquake nucleating above the weak mechanical layer. The area of the rupture is shown using a red–yellow gradient. An earthquake rupturing the total fault length (L) and the total thickness (W_{total}) above the weak layer would result in nonrealistic, highly elongated ruptures. In figure panel b, we propose a more realistic case: an earthquake offsetting the total thickness above the weak layer (W_{total}) and a rupture length weighted by the aspect ratio (L_w).

764

765

8. Seismic characterisation of active faults in the southwestern Valencia Trough.

In this section, we compute the seismic potential of the active faults in the southwestern Valencia Trough by applying several scaling relationships. We perform two distinct calculations corresponding to the two scenarios described earlier. i) In the first scenario, we assume a rupture involving both the supra- and subsalt successions. That is, this first scenario accounts for an earthquake rupturing the entire seismogenic crust. This scenario provides the maximum seismic potential of the faults. ii) In the second scenario, we assume that a rupture is restricted to the suprasalt succession. For this calculation, we apply several area-based scaling relationships, and we use the area weighted by the aspect ratio as the input parameter. Since the rupture area involved in this second scenario is relatively small, a relatively low seismogenic potential is expected.

8.1. First scenario: Ruptures involving the entire seismogenic crust.

For both scenarios, we apply the scaling relationships of Wells & Coppersmith (1994) (values corresponding to normal faults for the Cullera and Valencia faults, and to strike slip faults for the Albufera Fault) and Stirling et al. (2002). In the first scenario, i.e., ruptures involving the entire seismogenic crust, we assume that a complete fault ruptured from the subsalt basement through the suprasalt succession. To compute the seismogenic potential of this first scenario we used the fault length and fault area as the primary input parameter (Table 1). The fault area used for these calculations was the result of multiplying the fault length by the fault width. We prefer to use this simplification instead of the areas calculated from our 3D models to ensure consistency when comparing magnitude estimates derived from the methodology involving a correction factor (see below). The total thickness of the seismogenic crust in the study area is not precisely known. García-Mayordomo (2005) proposed a thickness ranging between 9 and 11 km. This value agrees with crust thicknesses based on deep seismic profiles (Etheve et al., 2016; Maillard & Mauffret, 2013; Ramos et al., 2025) as well as the lithospheric structure

based on P-wave receiver function analysis and seismic tomography (Mancilla et al., 2015; Palomeras et al., 2017).. Therefore, we assumed a mean thickness of the seismogenic crust of 10 km.

Table 1 Source parameters obtained from length- and area-based scaling relationships (Wells & Coppersmith, 1994 -WC94- and Stirling et al., 2002 -Stirling02-) assuming ruptures involving the entire seismogenic crust. L, fault length; M_w, moment magnitude; AD, average displacement; MD, maximum displacement. Values computed using length-based Wells & Coppersmith (1994) relationships refer to normal faulting (Cullera and Valencia faults) and strike-slip faulting (Albufera Fault).

	Length-based relationships						Area-based relationships		
		WC94			Stirling02			WC94	Stirling02
	L km	M_W	AD m	MD m	M_W	AD m	A km^2	M_W	M_W
Cullera Fault	59	7.2 ±0.34	1.61 ±0.37	4.94 ±0.41	7.3 ±0.30	2.39 ±0.24	834.4	6.91 ±0.25	7.22 ±0.26
Albufera Fault	40	6.97 ±0.34	0.99 ±0.37	2.75 ±0.41	7.16 ±0.30	2.23 ±0.24	565.7	6.74 ±0.25	7.1 ±0.26
Valencia Fault	20	6.58 ±0.34	0.42 ±0.37	0.97 ±0.41	6.92 ±0.30	1.97 ±0.24	282.9	6.43 ±0.25	6.88 ±0.26

8.2. Second scenario: Ruptures involving only the suprasalt succession

In this scenario, the presence of a mechanically weak layer within the seismogenic crust is considered to control the seismic potential of active faults. As discussed previously, we use the weighted rupture area as the input parameter for the scaling relationships. The weighting factor is based on the aspect ratio of normal faults. To provide context for this approach, we also present seismic parameters calculated from the total fault area offsetting the entire suprasalt succession. The aspect ratios

of normal fault ruptures vary widely (0.4–18); however, most of the observed ruptures are within the range of 0.5 to 3.5 (Nicol et al., 1996; Stock & Smith, 2000), with a mode value of 1.8 (30%, Stock & Smith, 2000). Numerical simulations of strike-slip faults by Weng & Yang (2016) demonstrated that the width of the seismogenic layer significantly influences the rupture aspect ratios. According to their findings, a seismogenic layer thickness of approximately 10 km marks a critical boundary: for thicknesses less than this value, rupture aspect ratios remain low (ca. 2), whereas thicknesses greater than 10 km result in significantly higher aspect ratios (<8). Considering these findings and given that the suprasalt succession in the southwestern Valencia Trough has an average thickness of approximately 5 km, we adopt an aspect ratio of 1.8 for our calculations.

In the southwestern Valencia Trough, the suprasalt succession thickness at the location of active faults varies. We used thicknesses of 5 km, 3.3 km and 2.3 km for the Cullera, Valencia, and Albufera faults respectively, as input values for our calculation. For events unrestricted by the aspect ratio (i.e., earthquakes rupturing the entire fault length and width of the suprasalt succession), we compute the rupture area as the product of length and width accounting also for the fault dip ($L*W/\sin\beta$). However, when the seismic potential for ruptures weighted by the aspect ratio is calculated, the controlling factor is the fault width.

Table 2 Moment magnitude obtained from scaling relationships (Wells & Coppersmith, 1994 -WC94- and Stirling et al., 2002 -Stirling02-). The first column (not weighted area) corresponds to the values obtained assuming ruptures involving the total suprasalt succession. The second column (weighted area) shows the values obtained using the area weighted by the aspect ratio as input parameter.

	Not weighted area			Weighted area		
	Input parameters A km^2	M_W WC94	M_W Stirling02	Input parameters A km^2	M_W WC94	M_W Stirling02
Cullera Fault	360	6.54 ±0.34	6.96 ±0. 26	67	5.79 ±0.34	6.42 ±0.26
Albufera Fault	112	6.02 ±0.34	6.59 ±0. 26	14	5.16 ±0.34	5.93 ±0.26
Valencia Fault	81	5.87 ±0.34	6.48 ±0. 26	29	5.42 ±0.34	6.16 ±0.26

The comparison between the standard application of earthquake source scaling relations and the approach presented here for regions characterised by the presence of a weak mechanical layer within the seismogenic crust reveals significant differences (Fig. 12). The maximum expected magnitudes for characteristic events rupturing the entire seismogenic crust (i.e., propagating across the basement–cover interface) are estimated to be 6.9–7.3, 6.4–6.9, and 6.7–7.2 for the Cullera, Valencia, and Albufera Faults, respectively. In contrast, for hypothetical earthquakes restricted to the suprasalt succession and rupturing of the total length of the faults, the expected magnitudes are lower, ranging from 6.54-6.96, 5.87-6.48, 6.02-6.59 for the Cullera, Valencia, and Albufera faults, respectively. However, in such cases, we argue that the seismic potential derived using area-weighted relations provides a more realistic estimate. Using this approach, our calculations yield maximum magnitudes of 5.79-6.42, 5.42-6.16, and 5.11-5.93 for the Cullera, Valencia, and Albufera faults, respectively. These values are 5-15 % lower than those obtained when accounting for the total suprasalt succession thickness.

When the area-weighted values are compared with the maximum expected magnitudes for ruptures involving the entire seismogenic crust, the results reveal a 11-26% reduction. This discrepancy highlights the importance of incorporating mechanical layering into seismic potential assessments in regions where weak

layers influence fault dynamics and rupture propagation. Furthermore, these differences in seismic potential should be addressed in probabilistic seismic hazard assessments.

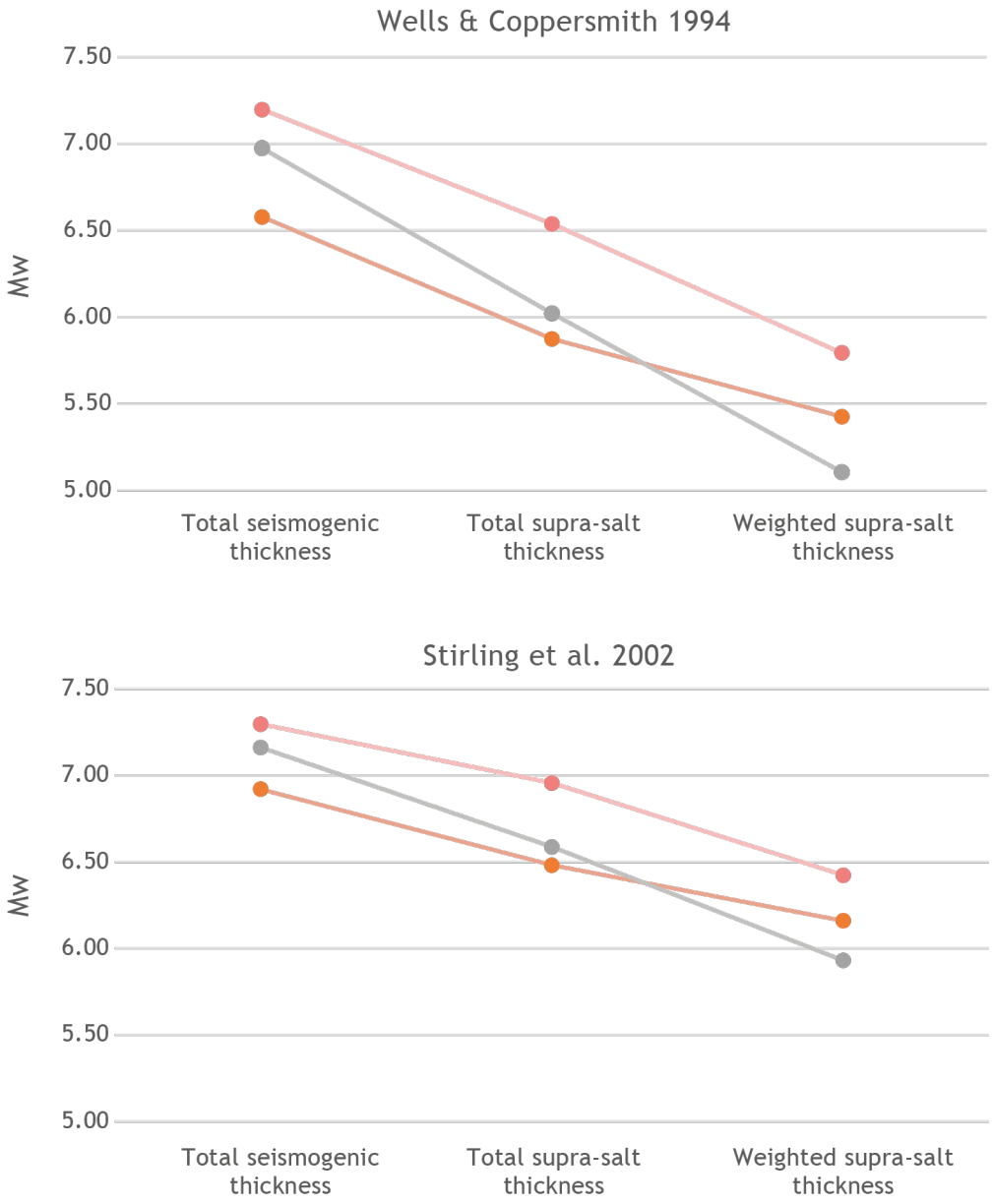

Figure 12. Plots of M_w values for the Cullera, Albufera and Valencia Faults obtained using the scaling relationships of Wells & Coppersmith (1994) and Stirling et al. (2002). The plots show the values computed assuming a rupture of the total seismogenic thickness, a rupture of the total suprasalt succession, and the values assuming a rupture of an area calculated using a suprasalt thickness weighted with the aspect ratio.

9. Conclusions

Analysis of a comprehensive subsurface dataset from the southwestern Valencia Trough enables the identification of three major active faults: the normal Cullera Fault, the oblique Albufera Fault, and the normal Valencia Fault. Among these faults, the Cullera Fault is the main active structure in this region, with a cumulative offset of 1800 m at the top of the Messinian marker. The long-term slip rate varies over time between 0.15 ±0.1 mm/y and 0.4 ±0.1 mm/y. The Albufera Fault, which is 55 km in length, has a long-term slip rate of 0.2 ±0.1 mm/y, whereas the 20-km-long Valencia Fault significantly influences the spatial distribution of Quaternary depocentres.

Our results also reveal a 10-km-thick heterogeneous seismogenic crust in the study area, largely because of a mechanically weak layer, which is composed mainly of Triassic evaporites. Consequently, two competing mechanisms are responsible for the offset along the active faults: tectonics and salt withdrawal. A quantitative evolutionary analysis of the Cullera Fault indicates that tectonics was the dominant mechanism during the Pliocene, whereas salt withdrawal took precedence in the early Quaternary (2.6–2 Ma). After 2 Ma, tectonic activity once again became the primary driver of fault displacement.

Using standard scaling relationships, we computed maximum expected magnitudes for the southwestern Valencia Trough faults. These maximum expected magnitudes range between 6.9-7.3 for the Cullera Fault, 6.7-7.2 for the Albufera Fault, and 6.4-6.9 for de Valencia Fault. However, the mechanically layered crust of the southwestern Valencia Trough influences seismicity: events may nucleate in either the basement or the suprasalt succession. Moreover, the weak layer could influence the vertical propagation of a potential rupture. That is, total or partial decoupling related to the mechanically weak layer implies that an earthquake that nucleated in the suprasalt succession would likely be restricted to this upper part of the seismogenic crust, yet larger events involving basement and cover units are also plausible. For reliable seismic hazard assessments, both scenarios must be accounted for. To compute the seismogenic potential of active faults under the assumption of rupture within the suprasalt succession, we propose the use of the

907 rupture aspect ratio as a correction factor for the maximum rupture area.
908 Specifically, the product of the suprasalt thickness (corrected by the fault dip) and
909 the fault length—weighted by the aspect ratio—provides a more realistic
910 approximation of the maximum rupture area. Using this method, the maximum
911 magnitudes for suprasalt ruptures of the southwestern Valencia Trough faults are
912 5.79-6.42, 5.42-6.16, and 5.11-5.93 for the Cullera, Valencia, and Albufera faults,
913 respectively. These values are 5-15% lower than those obtained by considering the
914 full suprasalt thickness alone, and 11-26% lower than estimates involving the entire
915 seismogenic crust.

916 Overall, these findings greatly enhance our understanding of the seismogenic
917 potential of the southwestern Valencia Trough, an offshore area near densely
918 populated areas. These findings provide a basis for improved seismic hazard
919 assessments. Additionally, as we are addressing offshore faults exhibiting vertical
920 displacement, our findings can be used to establish the tsunamigenic potential of
921 this region. Furthermore, this approach for incorporating mechanical
922 heterogeneities in the seismogenic crust can be applied to other regions and
923 tectonic settings with analogous structural configurations.

924

925

10. Author contribution

Martin-Rojas, I.: Conceptualization, Data curation, Formal analysis, Funding acquisition, Investigation, Methodology, Project administration, Supervision, Validation, Visualization, Writing – original draft preparation, review & editing

Ramos, A.; Data curation, Formal analysis, Funding acquisition, Investigation, Resources, Visualization, Writing – original draft preparation, review & editing

De Ruig, M.: Data curation, Formal analysis, Investigation, Resources, Visualization, Writing – original draft preparation, review & editing

Medina-Cascales, I.: Data curation, Formal analysis, Investigation, Visualization, Writing –review & editing

Santamaría-Pérez, E.: Data curation, Formal analysis, Investigation, Writing – review & editing

Alfaro, P.: Data curation, Formal analysis, Investigation, Supervision, Writing – review & editing

11. Competing interests

The authors declare that they have no conflict of interest.

12. Acknowledgements

We acknowledge the comments of the Raúl Pérez-López, an anonymous reviewer, and the Editor Solmaz Mohadjer, which significantly improved the quality of this paper.

13. Financial support

This research was funded by the Spanish Ministry of Science, Innovation and University (research projects PID2021-127967NB-I00 and RTI2018-100737-B-I00), Generalitat Valenciana (Valencian Regional Government, research projects AICO2021/196 and CIAPOS/2022/082, and University of Alicante (research project VIGROB053). The authors acknowledge the use of the MOVE Software Suite granted by PE Limited (Petex).

956 References

957 Agustí, J., Santos-Cubedo, A., Furió, M., De Marfá, R., Blain, H., Oms, O., & Sevilla, P.
958 (2011). The late Neogene-early Quaternary small vertebrate succession from the
959 Almenara-Casablanca karst complex (Castellón, Eastern Spain): Chronologic and
960 paleoclimatic context. *Quaternary International, 243*(1), 183–191.
961 10.1016/j.quaint.2010.11.016

962 Albarracín, S., Alcántara-Carrió, J., Barranco, A., Sánchez García, M. J., Fontán Bouzas, Á,
963 & Rey Salgado, J. (2013). Seismic evidence for the preservation of several stacked
964 Pleistocene coastal barrier/lagoon systems on the Gulf of Valencia continental shelf
965 (western Mediterranean). *Geo-Marine Letters, 33*(2-3), 217–223. 10.1007/s00367-
966 012-0315-x

967 Arche, A., & López-Gómez, J. (1996). Origin of the Permian-Triassic Iberian Basin, central-
968 eastern Spain. *Tectonophysics, 266*(1), 443–464. 10.1016/S0040-1951(96)00202-8

969 Barchi, M. R., Carboni, F., Michele, M., Ercoli, M., Giorgetti, C., Porreca, M., Azzaro, S., &
970 Chiaraluce, L. (2021). The influence of subsurface geology on the distribution of
971 earthquakes during the 2016-–2017 Central Italy seismic sequence. Tectonophysics,
972 807, 228797. https://doi.org/10.1016/j.tecto.2021.228797

973 Barchi, M. R., & Mirabella, F. (2009). The 1997–98 Umbria–Marche earthquake sequence:
974 “Geological” vs. “seismological” faults. Tectonophysics, 476(1–2), 170–179.
975 https://doi.org/10.1016/j.tecto.2008.09.013

976 Boncio, P., Lavecchia, G., & Pace, B. (2004). Defining a model of 3D seismogenic sources
977 for Seismic Hazard Assessment applications: The case of central Apennines (Italy).

978 Journal of Seismology, 8(3), 407–425.
979 https://doi.org/10.1023/B:JOSE.0000038449.78801.05

980 Buforn, E., & Udías, A. (2021). *El terremoto de Alcoy de 1620 y la serie sísmica de 1644 en*
981 *la comarca de Muro*. Centro Nacional de Información Geográfica.

982 Buforn, E., Udías, A., Sanz de Galdeano, C., & Cesca, S. (2015). The 1748 Montesa
983 (southeast Spain) earthquake — A singular event. *Tectonophysics, 664*, 139–153.
984 10.1016/j.tecto.2015.09.005

985 Cameselle, A. L., Urgeles, R., De Mol, B., Camerlenghi, A., & Canning, J. C. (2014). Late
986 Miocene sedimentary architecture of the Ebro Continental Margin (Western
987 Mediterranean): implications to the Messinian Salinity Crisis. *International Journal of*
988 *Earth Sciences : Geologische Rundschau, 103*(2), 423–440. 10.1007/s00531-013-
989 0966-5

990 Casciello, E., Vergés, J., Saura, E., Casini, G., Fernández, N., Blanc, E., Homke, S., & Hunt,
991 D. W. (2009). Fold patterns and multilayer rheology of the Lurestan Province, Zagros
992 simply folded belt (Iran). *Journal of the Geological Society, 166*(5), 947–959.
993 10.1144/0016-76492008-138

994 Cheng Jia, C. J., Rong, Y., Magistrale, H., Chen Guihua, C. G., & Xu Xiwei, X. X. (2019a).
995 Earthquake rupture scaling relations for mainland China. *Seismological Research*
996 *Letters, 91*(1), 248–261. 10.1785/0220190129

997 Cheng Jia, C. J., Rong, Y., Magistrale, H., Chen Guihua, C. G., & Xu Xiwei, X. X. (2019b).
998 Earthquake rupture scaling relations for mainland China. *Seismological Research*
999 *Letters, 91*(1), 248–261. 10.1785/0220190129

1000 Chiaraluce, L., Di Stefano, R., Tinti, E., Scognamiglio, L., Michele, M., Casarotti, E.,
1001 Cattaneo, M., De Gori, P., Chiarabba, C., Monachesi, G., Lombardi, A., Valoroso, L.,
1002 Latorre, D., & Marzorati, S. (2017). The 2016 Central Italy Seismic Sequence: A First
1003 Look at the Mainshocks, Aftershocks, and Source Models. Seismological Research
1004 Letters, 88(3), 757–771. https://doi.org/10.1785/0220160221

1005 Chiaraluce, L., Ellsworth, W. L., Chiarabba, C., & Cocco, M. (2003). Imaging the
1006 complexity of an active normal fault system: The 1997 Colfiorito (central Italy) case
1007 study. Journal of Geophysical Research: Solid Earth, 108(B6).
1008 https://doi.org/10.1029/2002JB002166

1009 Clavell, E., & Berastegui, X. (1991). Petroleum geology of the Gulf of Valencia. *Generation,*
1010 *Accumulation, and Production of Europe's Hydrocarbons,* , 355–368.
1011 https://www.scopus.com/inward/record.uri?eid=2-s2.0-
1012 0026310072&partnerID=40&md5=8f34c3d495738519a9101eb775a91bd4

1013 De Ruig, & M.J. (1992). *Tectono-sedimentary evolution of the Prebetic fold belt of Alicante*

1014 Del Rio, V. D., Rey, J., & Vegas, R. (1986). The Gulf of Valencia continental shelf:
1015 Extensional tectonics in Neogene and Quaternary sediments. *Marine Geology, 73*(1),
1016 169–179. 10.1016/0025-3227(86)90117-9

1017 DeMets, C., Gordon, R. G., Argus, D. F., & Stein, S. (1994). Effect of recent revisions to the
1018 geomagnetic reversal time scale on estimates of current plate motions. *Geophysical*
1019 *Research Letters, 21*(20), 2191–2194. 10.1029/94GL02118

1020 Duffy, O. B., Gawthorpe, R. L., & Docherty, M. (2023). Tectono-stratigraphic evolution of
1021 salt-influenced normal fault systems: an example from the Coffee-Soil Fault, Danish
1022 North Sea. *Journal of the Geological Society, 180*(6), 1. 10.1144/jgs2023-016

1023 Etheve, N., Frizon de Lamotte, D., Mohn, G., Martos, R., Roca, E., & Blanpied, C. (2016).
1024 Extensional vs contractional Cenozoic deformation in Ibiza (Balearic Promontory,
1025 Spain): Integration in the West Mediterranean back-arc setting. *Tectonophysics, 682*,
1026 35–55. 10.1016/j.tecto.2016.05.037

1027 Faccenna, C., Piromallo, C., Crespo-Blanc, A., Jolivet, L., & Rossetti, F. (2004a). Lateral
1028 slab deformation and the origin of the western Mediterranean arcs. *Tectonics*
1029 *(Washington, D.C.), 23*(1), np–n/a. 10.1029/2002TC001488

1030 Faccenna, C., Piromallo, C., Crespo-Blanc, A., Jolivet, L., & Rossetti, F. (2004b). Lateral
1031 slab deformation and the origin of the western Mediterranean arcs. *Tectonics*
1032 *(Washington, D.C.), 23*(1), np–n/a. 10.1029/2002TC001488

1033 Fang, P., Tugend, J., Mohn, G., Kusznir, N., & Ding, W. (2021a). Evidence for rapid large-
1034 amplitude vertical motions in the Valencia Trough (Western Mediterranean)
1035 generated by 3D subduction slab roll-back. *Earth and Planetary Science Letters, 575*,
1036 117179. 10.1016/j.epsl.2021.117179

1037 Fang, P., Tugend, J., Mohn, G., Kusznir, N., & Ding, W. (2021b). Evidence for rapid large-
1038 amplitude vertical motions in the Valencia Trough (Western Mediterranean)
1039 generated by 3D subduction slab roll-back. *Earth and Planetary Science Letters, 575*,
1040 117179. 10.1016/j.epsl.2021.117179

1041 Ford, M., Le Carlier de Veslud, C., & Bourgeois, O. (2007). Kinematic and geometric
1042 analysis of fault-related folds in a rift setting: The Dannemarie basin, Upper Rhine
1043 Graben, France. *Journal of Structural Geology, 29*(11), 1811–1830.
1044 10.1016/j.jsg.2007.08.001

García-Mayordomo, J., Insua-Arévalo, J. M., Martínez-Díaz, J. J., Jiménez-Díaz, A., Martín-Banda, R., Martín-Alfageme, S., Álvarez-Gómez, J. A., Rodríguez-Peces, M., Pérez-López, R., Rodríguez-Pascua, M. A., Masana, E., Perea, H., Martín-González, F., Giner-Robles, J., Nemser, E. S., & Cabral, J. (2012). The Quaternary active faults database of Iberia (QAFI v. 2.0). *Journal of Iberian Geology, 38*(1)10.5209/rev_JIGE.2012.v38.n1.39219

Gaspar-Escribano, J. M., Garcia-Castellanos, D., Roca, E., & Cloetingh, S. (2004). Cenozoic vertical motions of the Catalan Coastal Ranges (NE Spain): The role of tectonics, isostasy, and surface transport. *Tectonics (Washington, D.C.), 23*(1), np–n/a. 10.1029/2003TC001511

Geel, T. (1995). Oligocene to early Miocene tectono-sedimentary history of the Alicante region (SE Spain): implications for Western Mediterranean evolution. *Basin Research, 7*(4), 313–336. 10.1111/j.1365-2117.1995.tb00120.x

Geller, R. J. (1976). Scaling relations for earthquake source parameters and magnitudes. *Bulletin of the Seismological Society of America, 66*(5), 1501–1523. https://pubs.geoscienceworld.org/ssa/bssa/article/66/5/1501/117604

Godano, M., Larroque, C., Delouis, B., Ampuero, J., Arzu, F., Courboulex, F., Deschamps, A., van den Ende, M., Baize, S., & Ritz, J. (2025). Back to the Source: Connecting the Seismological Observations of Le Teil Earthquake (M_w 4.9, 2019/11/11, France) to the Local Geology. *Journal of Geophysical Research: Solid Earth*, *130*(9). https://doi.org/10.1029/2025JB03113

González, Á. (2017). The Spanish National Earthquake Catalogue: Evolution, precision and completeness. *Journal of Seismology, 21*(3), 435–471. 10.1007/s10950-016-9610-8

1068 Guimera, J., & Alvaro, M. (1990). Structure et évolution de la compression alpine dans la
1069 Chaîne ibérique et la Chaîne côtière catalane (Espagne). *Bulletin De La Société*
1070 *Géologique De France, 6*(2), 339–348. 10.2113/gssgfbull.VI.2.339

1071 Hongxing, G., & Anderson, J. K. (2007). Fault throw profile and kinematics of Normal fault:
1072 conceptual models and geologic examples. *Geological Journal of China Universities,*
1073 *13*(1), 75.

1074 Huang, J., Abrahamson, N. A., Sung, C., & Chao, S. (2024). New Empirical Source-Scaling
1075 Laws for Crustal Earthquakes Incorporating Fault Dip and Seismogenic-Thickness
1076 Effects. *Seismological Research Letters, 95*(4), 2352–2367. 10.1785/0220240034

1077 Hyndman, R. D., Yamano, M., & Oleskevich, D. A. (1997). The seismogenic zone of
1078 subduction thrust faults. *Island Arc, 6*(3), 244–260. 10.1111/j.1440-
1079 1738.1997.tb00175.x

1080 Improta, L., Latorre, D., Margheriti, L., Nardi, A., Marchetti, A., Lombardi, A. M., Castello,
1081 B., Villani, F., Ciaccio, M. G., Mele, F. M., Moretti, M., Battelli, P., Berardi, M.,
1082 Castellano, C., Melorio, C., Modica, G., Pirro, M., Rossi, A., Thermes, C., … Di Maro,
1083 R. (2019). Multi-segment rupture of the 2016 Amatrice-Visso-Norcia seismic
1084 sequence (central Italy) constrained by the first high-quality catalog of Early
1085 Aftershocks. Scientific Reports, 9(1), 6921. https://doi.org/10.1038/s41598-019-
1086 43393-2

1087 IGN. (2025). *Instituto Geográfico Nacional (2025) Servicio de Información Sísmica*.

1088 Jackson, C. A. -., & Rotevatn, A. (2013). 3D seismic analysis of the structure and evolution
1089 of a salt-influenced normal fault zone: A test of competing fault growth models.
1090 *Journal of Structural Geology, 54*, 215–234. 10.1016/j.jsg.2013.06.012

1091 Jackson, M. P. A., & Hudec, M. R. (2005). Stratigraphic record of translation down ramps in
1092 a passive-margin salt detachment. *Journal of Structural Geology, 27*(5), 889–911.
1093 10.1016/j.jsg.2005.01.010

1094 Jolivet, L., & Faccenna, C. (2000). Mediterranean extension and the Africa-Eurasia
1095 collision. *Tectonics, 19*(6), 1095–1106. 10.1029/2000TC900018

1096 Kanamori, H., & Anderson, D. L. (1975). Theoretical basis of some empirical relations in
1097 seismology. *Bulletin of the Seismological Society of America, 65*(5), 1073–1095.
1098 https://pubs.geoscienceworld.org/ssa/bssa/article/65/5/1073/117458

1099 Kane, K. E., Jackson, C. A. -., & Larsen, E. (2010). Normal fault growth and fault-related
1100 folding in a salt-influenced rift basin: South Viking Graben, offshore Norway. *Journal*
1101 *of Structural Geology, 32*(4), 490–506. 10.1016/j.jsg.2010.02.005

1102 Leonard, M. (2010). Earthquake fault scaling; self-consistent relating of rupture length,
1103 width, average displacement, and moment release. *Bulletin of the Seismological*
1104 *Society of America, 100*(5A), 1971–1988. 10.1785/0120090189

1105 Leonard, M. (2014). Self-consistent earthquake fault-scaling relations; update and
1106 extension to stable continental strike-slip faults. *Bulletin of the Seismological Society*
1107 *of America, 104*(6), 2953–2965. 10.1785/0120140087

1108 Lirer, F., Foresi, L. M., Iaccarino, S. M., Salvatorini, G., Turco, E., Cosentino, C., Sierro, F.
1109 J., & Caruso, A. (2019). Mediterranean Neogene planktonic foraminifer biozonation
1110 and biochronology. *Earth-Science Reviews, 196*, 102869.
1111 10.1016/j.earscirev.2019.05.013

1112 Lofi, J. (2011). *Seismic atlas of the "Messinian salinity crisis" markers in the Mediterranean*
1113 *and Black Seas*. Commission for the Geological Map of the World.

1114 Maillard, A., Mauffret, A., Watts, A. B., Torné, M., Pascal, G., Buhl, P., & Pinet, B. (1992).
1115 Tertiary sedimentary history and structure of the Valencia trough (western
1116 Mediterranean). *Tectonophysics, 203*(1), 57–75. 10.1016/0040-1951(92)90215-R

1117 Maillard, A., & Mauffret, A. (2013). Structure and present-day compression in the offshore
1118 area between Alicante and Ibiza Island (Eastern Iberian Margin). *Tectonophysics,*
1119 *591*, 116–130. 10.1016/j.tecto.2011.07.007

1120 Mansfield, C. S., & Cartwright, J. A. (1996). High resolution fault displacement mapping
1121 from three-dimensional seismic data: evidence for dip linkage during fault growth.
1122 *Journal of Structural Geology, 18*(2), 249–263. 10.1016/S0191-8141(96)80048-4

1123 Marsh, N., Imber, J., Holdsworth, R. E., Brockbank, P., & Ringrose, P. (2010). The structural
1124 evolution of the Halten Terrace, offshore Mid-Norway: extensional fault growth and
1125 strain localisation in a multi-layer brittle-ductile system. *Basin Research, 22*(2), 195–
1126 214. 10.1111/j.1365-2117.2009.00404.x

1127 Martí, J., Mitjavila, J., Roca, E., & Aparicio, A. (1992). Cenozoic magmatism of the valencia
1128 trough (western mediterranean): Relationship between structural evolution and
1129 volcanism. *Tectonophysics, 203*(1), 145–165. 10.1016/0040-1951(92)90221-Q

1130 Martínez-Solares, J. M., & Mezcua, J. (2002). *Catálogo sísmico de la Península Ibérica*.
1131 Madrid (Spain): Instituto Geográfico Nacional.

1132 Martinis, B., & Pieri, M. (1969). Alcune informazioni sulla formazione evaporitica del
1133 Triassico superiore nell'Italia centrale meridionale. Memorie Della Società Geologica
1134 Italiana, 4, 649–678.

1135 Maurin, J., & Niviere, B. (1999). Extensional forced folding and décollement of the pre-rift
1136 series along the Rhine graben and their influence on the geometry of the syn-rift
1137 sequences. *Forced Folds and Fractures* (pp. 73–86). The Geological Society of
1138 London. 10.1144/GSL.SP.2000.169.01.06

1139 McClusky, S., Reilinger, R., Mahmoud, S., Ben Sari, D., & Tealeb, A. (2003). GPS
1140 constraints on Africa (Nubia) and Arabia plate motions. *Geophysical Journal*
1141 *International, 155*(1), 126–138. 10.1046/j.1365-246X.2003.02023.x

1142 Michele, M., Chiaraluce, L., Di Stefano, R., & Waldhauser, F. (2020). Fine-Scale Structure
1143 of the 2016–2017 Central Italy Seismic Sequence From Data Recorded at the Italian
1144 National Network. Journal of Geophysical Research: Solid Earth, 125(4).
1145 https://doi.org/10.1029/2019JB018440

1146 Molinaro, M., Leturmy, P., Guezou, J. -., Frizon de Lamotte, D., & Eshraghi, S. A. (2005).
1147 The structure and kinematics of the southeastern Zagros fold-thrust belt, Iran: From
1148 thin-skinned to thick-skinned tectonics. *Tectonics, 24*(3), np–n/a.
1149 10.1029/2004TC001633

1150 Morley, C. K., Back, S., Van Rensbergen, P., Crevello, P., & Lambiase, J. J. (2003).
1151 Characteristics of repeated, detached, Miocene–Pliocene tectonic inversion events,
1152 in a large delta province on an active margin, Brunei Darussalam, Borneo. *Journal of*
1153 *Structural Geology, 25*(7), 1147–1169. 10.1016/S0191-8141(02)00130-X

1154 NEBOT, M., & GUIMERÀ, J. (2018). Kinematic evolution of a fold-and-thrust belt developed
1155 during basin inversion: the Mesozoic Maestrat basin, E Iberian Chain. *Geological*
1156 *Magazine, 155*(3), 630–640. 10.1017/S001675681600090X

1157 Nicol, A., Watterson, J., Walsh, J. J., & Childs, C. (1996). The shapes, major axis
1158 orientations and displacement patterns of fault surfaces. *Journal of Structural*
1159 *Geology, 18*(2), 235–248. 10.1016/S0191-8141(96)80047-2

1160 Nissen, E., Ghorashi, M., Jackson, J., Parsons, B., & Talebian, M. (2007). The 2005 Qeshm
1161 Island earthquake (Iran)—a link between buried reverse faulting and surface folding
1162 in the Zagros Simply Folded Belt? *Geophysical Journal International, 171*(1), 326–338.
1163 10.1111/j.1365-246X.2007.03514.x

1164 Nissen, E., Tatar, M., Jackson, J. A., & Allen, M. B. (2011). New views on earthquake
1165 faulting in the Zagros fold-and-thrust belt of Iran. *Geophysical Journal International,*
1166 *186*(3), 928–944. 10.1111/j.1365-246X.2011.05119.x

1167 Nocquet, J. -., & Calais, E. (2003). Crustal velocity field of western Europe from permanent
1168 GPS array solutions, 1996–2001. *Geophysical Journal International, 154*(1), 72–88.
1169 10.1046/j.1365-246X.2003.01935.x

1170 Nocquet, J. (2012). Present-day kinematics of the Mediterranean: A comprehensive
1171 overview of GPS results. *Tectonophysics, 579*, 220–242. 10.1016/j.tecto.2012.03.037

1172 Palano, M., González, P. J., & Fernández, J. (2015). The Diffuse Plate boundary of Nubia
1173 and Iberia in the Western Mediterranean: Crustal deformation evidence for viscous
1174 coupling and fragmented lithosphere. *Earth and Planetary Science Letters, 430*, 439–
1175 447. 10.1016/j.epsl.2015.08.040

1176 Pascal, G., Torné, M., Buhl, P., Watts, A. B., & Mauffret, A. (1992). Crustal and velocity
1177 structure of the Valencia trough (western Mediterranean), Part II. Detailed
1178 interpretation of five Expanded Spread Profiles. *Tectonophysics, 203*(1), 21–35.
1179 10.1016/0040-1951(92)90213-P

1180 Pascoe, R., Hooper, R., Storhaug, K., & Harper, H. (Jan 1, 1999). Evolution of extensional
1181 styles at the southern termination of the Nordland Ridge, Mid-Norway: a response to
1182 variations in coupling above Triassic salt. Paper presented at the *, 5*(1) 83–90.
1183 10.1144/0050083 https://www.lyellcollection.org/doi/10.1144/0050083

1184 Perea, H. (2006). *Falles actives i perillositat sísmica al marge nord-occidental del solc de*
1185 *València*

1186 Pérez-Peña, A., Martín-Davila, J., Gárate, J., Berrocoso, M., & Buforn, E. (2010). Velocity
1187 field and tectonic strain in Southern Spain and surrounding areas derived from GPS
1188 episodic measurements. *Journal of Geodynamics, 49*(3), 232–240.
1189 10.1016/j.jog.2010.01.015

1190 Ramos, A., Lopez-Mir, B., Wilson, E. P., Granado, P., & Muñoz, J. A. (2020). 3D
1191 reconstruction of syn-tectonic strata in a salt-related orogen: learnings from the Llert
1192 syncline (South-central Pyrenees). *Acta Geologica Hispanica, 18*(1), 1–19.
1193 10.1344/GeologicaActa2020.18.20

1194 Ramos, A., de Ruig, M. J., Pedrera, A., Alfaro, P., & Martin-Rojas, I. (2025). Salt expulsion
1195 triggered by prograding clinoforms in the SW Valencia Trough (SE Spain). *Marine and*
1196 *Petroleum Geology, 173*, 107268. 10.1016/j.marpetgeo.2024.107268

1197 Ramos, A., Pedrera, A., García-Senz, J., López-Mir, B., & Salas, R. (2023). Seismic
1198 evidence for ductile necking of the mid-lower crust beneath the Columbrets Basin

(Western Mediterranean). *Terra Nova (Oxford, England), 35*(5), 404–412. 10.1111/ter.12664

Rehault, J., Boillot, G., & Mauffret, A. (1984). The Western Mediterranean Basin geological evolution. *Marine Geology, 55*(3), 447–477. 10.1016/0025-3227(84)90081-1

Ribó, M., Puig, P., Muñoz, A., Lo Iacono, C., Masqué, P., Palanques, A., Acosta, J., Guillén, J., & Gómez Ballesteros, M. (2016a). Morphobathymetric analysis of the large fine-grained sediment waves over the Gulf of Valencia continental slope (NW Mediterranean). *Geomorphology, 253*, 22–37. 10.1016/j.geomorph.2015.09.027

Ribó, M., Puig, P., Urgeles, R., Van Rooij, D., & Muñoz, A. (2016b). Spatio-temporal evolution of sediment waves developed on the Gulf of Valencia margin (NW Mediterranean) during the Plio-Quaternary. *Marine Geology, 378*, 276–291. 10.1016/j.margeo.2015.11.011

Richardson, N. J., Underhill, J. R., & Lewis, G. (2005). The role of evaporite mobility in modifying subsidence patterns during normal fault growth and linkage, Halten Terrace, Mid-Norway. *Basin Research, 17*(2), 203–223. 10.1111/j.1365-2117.2005.00250.x

Roca, E. (1994). La evolución geodinámica de la Cuenca Catalano-Balear y áreas adyacentes desde el Mesozoico hasta la actualidad. *Acta Geologica Hispanica, 29*(1), 3–25. https://raco.cat/index.php/ActaGeologica/article/view/75462

Roca, E. (2001). The Northwest Mediterranean Basin (Valencia Trough, Gulf of Lions and Liguro-Provencal basins): structure and geodynamic evolution. *Mem. Mus. Natl. Hist. Nat. (France)* (pp. 671–706)

1221 Roca, E., Frizon de Lamotte, D., Mauffret, A., Bracene, R., Verges, J., Benaouali, N.,
1222 Fernandez, M., Munoz, J. A., & Zeyen, H. (2004). TRANSMED-transect II (Aquitaine
1223 basin, Pyrenees, Ebro basin, Catalan coastal ranges, Valancia trough, Balearic
1224 promontory, Algerian basin, Tell, Sahara Atlas, Sahara platform). In : W. Cavazza, F.
1225 Roure, W. Spakman, G.M. Stampfli and P.A. Ziegler (Eds). The TRANSMED Atlas - the
1226 Mediterranean region from Crust to Mantle. *Springer, Berlin* https://hal.science/hal-
1227 00069583

1228 Roca, E., & Desegaulx, P. (1992). Analysis of the geological evolution and vertical
1229 movements in the València Trough area, western Mediterranean. *Marine and*
1230 *Petroleum Geology, 9*(2), 167,IN1,177–176,IN8,185. 10.1016/0264-8172(92)90089-W

1231 Roca, E., & Guimerà, J. (1992). The Neogene structure of the eastern Iberian margin:
1232 Structural constraints on the crustal evolution of the Valencia trough (western
1233 Mediterranean). *Tectonophysics, 203*(1), 203–218. 10.1016/0040-1951(92)90224-T

1234 Roca, E., Sans, M., Cabrera, L., & Marzo, M. (1999). Oligocene to Middle Miocene
1235 evolution of the central Catalan margin (northwestern Mediterranean).
1236 *Tectonophysics, 315*(1), 209–229. 10.1016/S0040-1951(99)00289-9

1237 Rouby, D., Guillocheau, F., Robin, C., Bouroullec, R., Raillard, S., Castelltort, S., & Nalpas,
1238 T. (2003). Rates of deformation of an extensional growth fault/raft system (offshore
1239 Congo, West African margin) from combined accommodation measurements and 3-
1240 D restoration. *Basin Research, 15*(2), 183–200. 10.1046/j.1365-2117.2003.00200.x

1241 Roustaei, M., Nissen, E., Abbassi, M., Gholamzadeh, A., Ghorashi, M., Tatar, M., Yamini-
1242 Fard, F., Bergman, E., Jackson, J., & Parsons, B. (2010). The 2006 March 25 Fin
1243 earthquakes (Iran)—insights into the vertical extents of faulting in the Zagros Simply

Folded Belt. *Geophysical Journal International, 181*(3), 1275–1291. 10.1111/j.1365-246X.2010.04601.x

Rovida, A., Locati, M., Camassi, R., Lolli, B., & Gasperini, P. (2020). The Italian earthquake catalogue CPTI15. Bulletin of Earthquake Engineering, 18(7), 2953–2984. https://doi.org/10.1007/s10518-020-00818-y

Ruff, L., & Kanamori, H. (1983). Seismic coupling and uncoupling at subduction zones. *Tectonophysics, 99*(2), 99–117. 10.1016/0040-1951(83)90097-5

Ruig, M. J. d. (1996). Extensional diapirism in the eastern Prebetic foldbelt, southeastern Spain. *AAPG Memoir,* (65) https://www.osti.gov/biblio/585188

Sàbat, F., Gelabert, B., Rodríguez-Perea, A., & Giménez, J. (2011). Geological structure and evolution of Majorca: Implications for the origin of the Western Mediterranean. *Tectonophysics, 510*(1), 217–238. 10.1016/j.tecto.2011.07.005

Salas, R., Guimera, J., Mas, R., Martin-Closas, C., Melendez, A., & Alonso, A. (2001a). Evolution of the Mesozoic Central Iberian Rift System and its Cainozoic inversion (Iberian chain). *Mémoires Du Muséum National D'histoire Naturelle (1993), 186*, 145–186.

Salas, R., Guimera, J., Mas, R., Martin-Closas, C., Melendez, A., & Alonso, A. (2001b). Evolution of the Mesozoic Central Iberian Rift System and its Cainozoic inversion (Iberian chain). *Mémoires Du Muséum National D'histoire Naturelle (1993), 186*, 145–186.

1264 Seranne, M. (1999). The Gulf of Lion continental margin (NW Mediterranean) revisited by
1265 IBS: an overview. *Geological Society special publication* (pp. 15–36). The Geological
1266 Society of London. 10.1144/GSL.SP.1999.156.01.03

1267 Serpelloni, E., Vannucci, G., Pondrelli, S., Argnani, A., Casula, G., Anzidei, M., Baldi, P., &
1268 Gasperini, P. (2007). Kinematics of the Western Africa-Eurasia plate boundary from
1269 focal mechanisms and GPS data. *Geophysical Journal International, 169*(3), 1180–
1270 1200. 10.1111/j.1365-246X.2007.03367.x

1271 Sherkati, S., Molinaro, M., Frizon de Lamotte, D., & Letouzey, J. (2005). Detachment
1272 folding in the Central and Eastern Zagros fold-belt (Iran): salt mobility, multiple
1273 detachments and late basement control. *Journal of Structural Geology, 27*(9), 1680–
1274 1696. 10.1016/j.jsg.2005.05.010

1275 Soler y José, R., Martínez del Olmo, W., Megías, A. G., & Abeger Monteagudo, J. A. (1983).
1276 Rasgos básicos del neógeno del Mediterráneo español. *Mediterránea. Serie de*
1277 *Estudios Geológicos, 1*, 71–82.

1278 Stampfli, G. M., & Hocker, C. F. W. (1989). Messinian palaeorelief from a 3-D seismic
1279 survey in the Tarraco concession area (Spanish Mediterranean Sea). *Geologie En*
1280 *Mijnbouw, 68*(2), 201–210.

1281 Stewart, S. A., Ruffell, A. H., & Harvey, M. J. (1997). Relationship between basement-linked
1282 and gravity-driven fault systems in the UKCS salt basins. *Marine and Petroleum*
1283 *Geology, 14*(5), 581–604. 10.1016/S0264-8172(97)00008-1

1284 Stich, D., Martín, R., & Morales, J. (2010). *Moment tensor inversion for Iberia-Maghreb*
1285 *earthquakes 2005-2008*. Elsevier.

1286 Stich, D., Serpelloni, E., de Lis Mancilla, F., & Morales, J. (2006). Kinematics of the Iberia–
1287 Maghreb plate contact from seismic moment tensors and GPS observations.
1288 *Tectonophysics, 426*(3), 295–317. 10.1016/j.tecto.2006.08.004

1289 Stirling, M., Goded, T., Berryman, K., & Litchfield, N. (2013). Selection of earthquake
1290 scaling relationships for seismic-hazard analysis. *Bulletin of the Seismological*
1291 *Society of America, 103*(6), 2993–3011. 10.1785/0120130052

1292 Stirling, M., Rhoades, D., & Berryman, K. (2002). Comparison of earthquake scaling
1293 relations derived from data of the instrumental and preinstrumental era. *Bulletin of*
1294 *the Seismological Society of America, 92*(2), 812–830. 10.1785/0120000221

1295 Stock, C., & Smith, E. G. C. (2000). Evidence for different scaling of earthquake source
1296 parameters for large earthquakes depending on faulting mechanism. *Geophysical*
1297 *Journal International, 143*(1), 157–162. 10.1046/j.1365-246x.2000.00225.x

1298 Thorsen, C. E. (1963). Age of growth faulting in southeast Louisiana.

1299 Torné, M., Pascal, G., Buhl, P., Watts, A. B., & Mauffret, A. (1992). Crustal and velocity
1300 structure of the Valencia trough (western Mediterranean), Part I. A combined
1301 refraction/ wide-angle reflection and near-vertical reflection study. *Tectonophysics,*
1302 *203*(1), 1–20. 10.1016/0040-1951(92)90212-O

1303 Tvedt, A. B. M., Rotevatn, A., Jackson, C. A. -., Fossen, H., & Gawthorpe, R. L. (2013).
1304 Growth of normal faults in multilayer sequences: A 3D seismic case study from the
1305 Egersund Basin, Norwegian North Sea. *Journal of Structural Geology, 55*, 1–20.
1306 10.1016/j.jsg.2013.08.002

1307 Valoroso, L., Chiaraluce, L., Piccinini, D., Di Stefano, R., Schaff, D., & Waldhauser, F.
1308 (2013). Radiography of a normal fault system by 64,000 high-precision earthquake
1309 locations: The 2009 L'Aquila (central Italy) case study. Journal of Geophysical
1310 Research: Solid Earth, 118(3), 1156–1176. https://doi.org/10.1002/jgrb.50130

1311 van Hinsbergen, D. J. J., Torsvik, T. H., Schmid, S. M., Maţenco, L. C., Maffione, M.,
1312 Vissers, R. L. M., Gürer, D., & Spakman, W. (2020). Orogenic architecture of the
1313 Mediterranean region and kinematic reconstruction of its tectonic evolution since the
1314 Triassic. *Gondwana Research, 81*, 79–229. 10.1016/j.gr.2019.07.009

1315 van Hinsbergen, D. J. J., Vissers, R. L. M., & Spakman, W. (2014). Origin and consequences
1316 of western Mediterranean subduction, rollback, and slab segmentation. *Tectonics*
1317 *(Washington, D.C.), 33*(4), 393–419. 10.1002/2013TC003349

1318 Vargas, H., Gaspar-Escribano, J. M., López-Gómez, J., Van Wees, J., Cloetingh, S., de La
1319 Horra, R., & Arche, A. (2009). A comparison of the Iberian and Ebro Basins during the
1320 Permian and Triassic, eastern Spain: A quantitative subsidence modelling approach.
1321 *Tectonophysics, 474*(1), 160–183. 10.1016/j.tecto.2008.06.005

1322 Verges, J., & Sabat, F. (1999). Constraints on the Neogene Mediterranean kinematic
1323 evolution along a 1000 km transect from Iberia to Africa. *Geological Society special*
1324 *publication* (pp. 63–80). The Geological Society of London.
1325 10.1144/GSL.SP.1999.156.01.05

1326 Verges, J., & Fernandez, M. (2012). Tethys–Atlantic interaction along the Iberia–Africa
1327 plate boundary: The Betic–Rif orogenic system. *Tectonophysics, 579*, 144–172.
1328 10.1016/j.tecto.2012.08.032

Wells, D. L., & Coppersmith, K. J. (1994). New empirical relationships among magnitude, rupture length, rupture width, rupture area, and surface displacement. *Bulletin of the Seismological Society of America, 84*(4), 974–1002. https://pubs.geoscienceworld.org/ssa/bssa/article/84/4/974/119792

Weng, H., & Yang, H. (2017). Seismogenic width controls aspect ratios of earthquake ruptures. *Geophysical Research Letters, 44*(6), 2725–2732. 10.1002/2016gl072168

Withjack, M. O., & Callaway, S. (2000). Active normal faulting beneath a salt layer; an experimental study of deformation patterns in the cover sequence. *AAPG Bulletin, 84*(5), 627–651. 10.1306/C9EBCE73-1735-11D7-8645000102C1865D

Withjack, M. O., Olson, J., & Peterson, E. (1990). Experimental models of extensional forced folds. *AAPG Bulletin, 74*(7), 1038–1054. 10.1306/0C9B23FD-1710-11D7-8645000102C1865D

Yen, Y., & Ma, K. (2011a). Source-scaling relationship for M 4.6-8.9 earthquakes, specifically for earthquakes in the collision zone of Taiwan. *Bulletin of the Seismological Society of America, 101*(2), 464–481. 10.1785/0120100046

Yen, Y., & Ma, K. (2011b). Source-scaling relationship for M 4.6-8.9 earthquakes, specifically for earthquakes in the collision zone of Taiwan. *Bulletin of the Seismological Society of America, 101*(2), 464–481. 10.1785/0120100046

Zazo, C. (1979). El problema del límite Plio-Pleistoceno en el litoral S y SE de España. *Trabajos N/Q, 9*, 65–72.

1351